

MAM-2201, a synthetic cannabinoid drug of abuse, suppresses the synaptic input to cerebellar Purkinje cells via activation of presynaptic CB1 receptors



Tomohiko Irie^{a,*}, Ruri Kikura-Hanajiri^b, Makoto Usami^a, Nahoko Uchiyama^b,
Yukihiro Goda^c, Yuko Sekino^{a,**}

^a Division of Pharmacology, National Institute of Health Sciences, Tokyo, Japan

^b Division of Pharmacognosy, Phytochemistry, and Narcotics, National Institute of Health Sciences, Tokyo, Japan

^c Division of Drugs, National Institute of Health Sciences, Tokyo, Japan

ARTICLE INFO

Article history:

Received 26 June 2014

Received in revised form

18 December 2014

Accepted 20 February 2015

Available online 5 March 2015

Keywords:

Synthetic cannabinoids

MAM-2201

Cannabinoid receptor type 1

Purkinje cell

Cerebellum

Neurotransmitter release

ABSTRACT

Herbal products containing synthetic cannabinoids—initially sold as legal alternatives to marijuana—have become major drugs of abuse. Among the synthetic cannabinoids, [1-(5-fluoropentyl)-1H-indol-3-yl](4-methyl-1-naphthalenyl)-methanone (MAM-2201) has been recently detected in herbal products and has psychoactive and intoxicating effects in humans, suggesting that MAM-2201 alters brain function. Nevertheless, the pharmacological actions of MAM-2201 on cannabinoid receptor type 1 (CB1R) and neuronal functions have not been elucidated. We found that MAM-2201 acted as an agonist of human CB1Rs expressed in AtT-20 cells. In whole-cell patch-clamp recordings made from Purkinje cells (PCs) in slice preparations of the mouse cerebellum, we also found that MAM-2201 inhibited glutamate release at parallel fiber-PC synapses via activation of presynaptic CB1Rs. MAM-2201 inhibited neurotransmitter release with an inhibitory concentration 50% of 0.36 μ M. MAM-2201 caused greater inhibition of neurotransmitter release than Δ^9 -tetrahydrocannabinol within the range of 0.1–30 μ M and JWH-018, one of the most popular and potent synthetic cannabinoids detected in the herbal products, within the range of 0.03–3 μ M. MAM-2201 caused a concentration-dependent suppression of GABA release onto PCs. Furthermore, MAM-2201 induced suppression of glutamate release at climbing fiber-PC synapses, leading to reduced dendritic Ca^{2+} transients in PCs. These results suggest that MAM-2201 is likely to suppress neurotransmitter release at CB1R-expressing synapses in humans. The reduction of neurotransmitter release from CB1R-containing synapses could contribute to some of the symptoms of synthetic cannabinoid intoxication including impairments in cerebellum-dependent motor coordination and motor learning.

© 2015 Elsevier Ltd. All rights reserved.

Abbreviations: ACSF, artificial cerebrospinal fluid; AM251, N-(piperidin-1-yl)-5-(4-iodophenyl)-1-(2,4-dichlorophenyl)-4-methyl-1H-pyrazole-3-carboxamide; CB1R, cannabinoid receptor type 1; CB2R, cannabinoid receptor type 2; CF, climbing fiber; CI, confidence interval; CV, coefficient of variation; DNQX, 6,7-dinitroquinoxaline-2,3-dione; EC50, effective concentration 50%; eCBs, endocannabinoids; EGTA, ethylene glycol tetraacetic acid; EPSC, excitatory postsynaptic current; GFP, green fluorescent protein; hCB1R, human CB1R; HEPES, 4-(2-hydroxyethyl)-1-piperazineethanesulfonic acid; IC50, inhibitory concentration 50%; IEL, inter-event interval; IPSC, inhibitory postsynaptic current; JWH-018, naphthalen-1-yl-(1-pentylindol-3-yl)methanone; LTD, long-term depression; MAM-2201, [1-(5-fluoropentyl)-1H-indol-3-yl](4-methyl-1-naphthalenyl)-methanone; mCB1R, mouse CB1R; mIPSC, miniature IPSC; OGB-1, Oregon Green 488 BAPTA-1 hexapotassium salt; P, postnatal day; PC, Purkinje cell; PF, parallel fiber; PPR, paired-pulse ratio; qEPSC, quantal EPSC; THC, tetrahydrocannabinol; TTX, tetrodotoxin; WIN, WIN 55,212-2 mesylate, (R)-(+)-[2,3-Dihydro-5-methyl-3-(4-morpholinylmethyl)pyrrolo[1,2,3-de]-1,4-benzoxazin-6-yl]-1-naphthalenylmethanone mesylate.

* Corresponding author. Division of Pharmacology, National Institute of Health Sciences, 1-18-1 Kamiyoga, Setagaya-ku, Tokyo 158-8501, Japan. Tel.: +81 3 3700 9762.

** Corresponding author. Division of Pharmacology, National Institute of Health Sciences, 1-18-1 Kamiyoga, Setagaya-ku, Tokyo 158-8501, Japan. Tel.: +81 3 3700 9692.

E-mail addresses: irie@nihs.go.jp (T. Irie), yukos@nihs.go.jp (Y. Sekino).

<http://dx.doi.org/10.1016/j.neuropharm.2015.02.025>

0028-3908/© 2015 Elsevier Ltd. All rights reserved.

1. Introduction

Marijuana (*Cannabis sativa*) has been widely abused for recreational purposes and contains the psychoactive compound Δ^9 -tetrahydrocannabinol (Δ^9 -THC) (Taura et al., 2007). Δ^9 -THC binds to cannabinoid receptors type 1 and 2 (CB1R and CB2R), which are G protein-coupled receptors. CB1Rs are abundantly expressed in the mammalian brain, whereas CB2Rs are expressed mainly in the immune system (Showalter et al., 1996; Mackie, 2008; Kano et al., 2009). The psychoactive effects of Δ^9 -THC are mediated by CB1Rs (Huestis et al., 2001; Monory et al., 2007). Starting in the late 2000s, herbal products containing synthetic cannabinoids, which are chemical compounds produced for the purpose of mimicking the effects of Δ^9 -THC, became a major class of drugs of abuse, and are sold as alternatives to marijuana around the world (Auwarter et al., 2009; Vardakou et al., 2010; Seely et al., 2012; Kikura-Hanajiri et al., 2013). Among the synthetic cannabinoids, [1-(5-fluoropentyl)-1H-indol-3-yl](4-methyl-1-naphthalenyl)-methanone (MAM-2201, Fig. 1A) was recently identified in these herbal products (Moosmann et al., 2012; Derungs et al., 2013; Kikura-Hanajiri et al., 2013; Saito et al., 2013; Uchiyama et al., 2013; Lonati et al., 2014). In humans, abuse of products containing MAM-2201 causes a psychotic state with agitation, aggression, and anxiety, and can cause serious harm to the user including death. These reports imply that MAM-2201 exerts potent pharmacological actions on brain functions and causes psychoactive and intoxicating effects. Nevertheless, it remains unknown whether MAM-2201 activates CB1Rs and how MAM-2201 affects neuronal functions such as synaptic transmission.

Endocannabinoids (eCBs) mediate various types of synaptic plasticity throughout the mammalian brain. eCBs are released from postsynaptic neurons in response to synaptic activity and act in a retrograde manner on presynaptic terminals, to suppress neurotransmitter release (Wilson and Nicoll, 2002; Kano et al., 2009; Regehr et al., 2009). The synaptic effects of eCBs are mediated by presynaptic CB1Rs. In presynaptic terminals, activation of CB1Rs mainly inhibits voltage-gated Ca^{2+} channels coupled to exocytosis, leading to a reduction of neurotransmitter release (Brown et al., 2004; Kushmerick et al., 2004).

Numerous neurophysiological and neuropharmacological studies of CB1Rs have been performed on the cerebellum of rodents, which have well-characterized neuronal circuits and play crucial roles in motor coordination and motor learning (Llinas et al., 2004; Kano et al., 2009). In the cerebellum, Purkinje cells (PCs) are the principal GABAergic neurons and provide the sole output from the cerebellar cortex. PCs receive two types of glutamatergic excitatory inputs, climbing fibers (CFs) and parallel fibers (PFs). CFs arise from the inferior olivary complex. Activation of CF-PC synapses induces strong postsynaptic depolarization, which evokes a

dendritic Ca^{2+} transient and complex spikes consisting of a burst of several action potentials (spikelets). PFs are the axons of the granule cells located in the deep layers of the cerebellum and form numerous *en passant* synapses on the spines of distal dendrites of PCs (Llinas et al., 2004). PCs also receive feed-forward inhibition from GABAergic interneurons in the molecular layer of the cerebellar cortex (Mittmann et al., 2005). Neurotransmitter release at CF-PC, PF-PC, and interneuron-PC synapses is suppressed via activation of presynaptic CB1Rs (Kreitzer and Regehr, 2001; Diana et al., 2002; Szabo et al., 2004; Kawamura et al., 2006; Safo et al., 2006). *In vivo* administration of synthetic CB1R agonists in mice impairs cerebellum-dependent motor coordination (DeSanty and Dar, 2001; Patel and Hillard, 2001). Thus, the effects of CB1R agonists on cerebellar functions are well understood. Therefore, the cerebellum is the ideal neuronal circuit to examine the potency of synthetic cannabinoids, whose actions on neuronal functions have not been determined.

Here, using whole-cell patch-clamp recordings, we investigated activity of MAM-2201 in human CB1R (hCB1R)-expressing AtT-20 cells, and then the effects of MAM-2201 on synaptic transmission in slice preparations of the mouse cerebellum. We found that MAM-2201 acted as an agonist of hCB1Rs and inhibited excitatory transmitter release at PF-PC synapses via activation of presynaptic CB1Rs. MAM-2201 decreased the synaptic transmission more strongly than Δ^9 -THC within the range of 0.1–30 μM and naphthalen-1-yl-(1-pentylindol-3-yl)methanone [JWH-018, Fig. 1B, one of the most popular and potent synthetic cannabinoids detected in the herbal products (Atwood et al., 2010)], within the range of 0.03–3 μM . Furthermore, MAM-2201 induced presynaptic suppression of CF-PC synapses, leading to a reduction in the number of spikelets in complex spikes and to attenuated dendritic Ca^{2+} transients in PCs.

2. Materials and methods

2.1. Cannabinoid-related compounds

MAM-2201 (Fig. 1A) and JWH-018 (Fig. 1B) were purchased from Cayman Chemical (Ann Arbor, MI, USA). (R)-(-)-[2,3-Dihydro-5-methyl-3-(4-morpholinylmethyl)pyrrolo[1,2,3-de]-1,4-benzoxazin-6-yl]-1-naphthalenylmethanone mesylate [WIN55,212-2 (WIN), a CB1R and CB2R agonist] and N-(Piperidin-1-yl)-5-(4-iodophenyl)-1-(2,4-dichlorophenyl)-4-methyl-1H-pyrazole-3-carboxamide (AM251, a CB1R antagonist) were purchased from Wako Pure Chemical Industries (Osaka, Japan) and Tocris Bioscience (Bristol, UK), respectively. Δ^9 -THC was purchased from Cerilliant (Round Rock, TX, USA). These compounds were dissolved in dimethylsulfoxide as stock solutions. In electrophysiological recordings from AtT-20 cells and from cerebellar PCs, the final concentrations of dimethylsulfoxide in extracellular solutions were maintained at 0.1 and 0.3% (v/v), respectively. WIN was used as a positive control, because WIN has been used in many studies to suppress neurotransmitter release at PF-, CF-, and interneuron-PC synapses via activation of presynaptic CB1Rs (Kreitzer and Regehr, 2001; Diana et al., 2002; Safo and Regehr, 2005; Kawamura et al., 2006).

2.2. Heterologous expression of CB1R in AtT-20 cells

AtT-20 cells were obtained from JCRB Cell Bank (Osaka, Japan) and were maintained in Ham's F-10 medium (GIBCO, Grand Island, NY) supplemented with 10% horse serum (GIBCO), 2.5% fetal bovine serum (GIBCO), and a mixture of penicillin and streptomycin solution (100 unit/mL and 100 mg/mL, respectively; GIBCO) in a 5% CO_2 incubator at 37 °C. The cells were plated onto grass coverslips coated with poly-D-lysine (Sigma-Aldrich, St Louis, MO) for gene transfection. hCB1R (SC111611; Origene, Rockville, MD; NCBI Reference Sequence: NM_016083.3) (Bruno et al., 2014) or mouse CB1R (mCB1R, MC206086; Origene; GenBank: BC079564.1) cDNAs, and green fluorescent protein (GFP) vector were cotransfected into the cells in a 9:1 M ratio using Lipofectamine LTX (Invitrogen, Carlsbad, CA) according to the manufacturer's instructions. Fluorescence of GFP was regarded as an indicator of transfected cells. Whole-cell patch-clamp recordings were made from the GFP-positive cells 20–48 h after transfection. The expression of CB1R proteins was confirmed by immunostaining with the combination of rabbit polyclonal anti-CB1R antibody (1:2000 dilution, CB1-Rb-Af380, Frontier Institute, Hokkaido, Japan) and AlexaFluor 568-conjugated goat anti-rabbit IgG secondary antibody (5 $\mu\text{g}/\text{mL}$, A-11011; Invitrogen) according to the methods described previously (Irie et al., 2014).

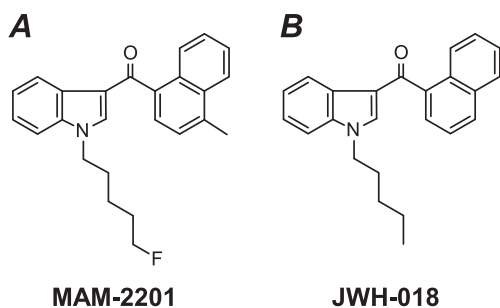


Fig. 1. The chemical structures of [1-(5-fluoropentyl)-1H-indol-3-yl](4-methyl-1-naphthalenyl)-methanone (MAM-2201, A) and naphthalen-1-yl-(1-pentylindol-3-yl)methanone (JWH-018, B).

The immunofluorescence signal was observed under a confocal microscope (A1R; Nikon, Tokyo, Japan; Fig. 2A).

2.3. Electrophysiological recordings from AtT-20 cells

AtT-20 cells were transferred to a recording chamber and continuously perfused at 2 mL/min with high-K⁺ extracellular solution containing (in mM): 87 NaCl, 60 KCl, 2 CaCl₂, 1 MgCl₂, 10 D-glucose, and 10 4-(2-hydroxyethyl)-1-piperazineethanesulfonic acid (HEPES) (pH adjusted to 7.4 with NaOH). The concentration of KCl was raised compared to normal extracellular solution to increase amplitudes of inwardly rectifier potassium currents (Mackie et al., 1995). All experiments were performed at 25 ± 1 °C. The cells were visualized by Nomarski optics and a near infrared-CCD camera (C3077-79; Hamamatsu Photonics, Hamamatsu, Japan) with a 40 × 0.8 NA numerical aperture water-immersion objective lens (Olympus, Tokyo, Japan) on an upright microscope (BX51WI; Olympus). GFP-positive cells were visualized and selected using epifluorescence optics (Olympus).

Patch pipettes were made from borosilicate glass capillaries (GC150F-100; Harvard Apparatus, Holliston, MA) and had a resistance of 3–5 MΩ when filled with a potassium gluconate-based internal solution containing (in mM): 125 K-gluconate, 10 KCl, 3 MgCl₂, 0.1 ethylene glycol tetraacetic acid (EGTA), 5 Na₂-ATP, 5 Na₂-phosphocreatine, 0.3 Na₂-GTP, and 10 HEPES (pH adjusted to 7.3 with KOH). Whole-cell patch-clamp recordings were performed from GFP-positive cells, and inward currents were evoked by applying voltage steps from a holding potential of –25 mV to –110 mV for 200 ms in voltage-clamp conditions. Membrane capacitance was calculated from the transient current evoked by applying a small voltage step (–5 mV, 20 ms duration) from a holding potential of –25 mV (Irie et al., 2006). Series resistance was compensated electronically by 70–90%, and the liquid junction potential (–5 mV) was corrected off-line.

Data were collected with Molecular Devices (Sunnyvale, CA) hardware and software (Multiclamp 700B, Digidata 1440A, Clampex 10.3) as described previously (Irie et al., 2014), and analyzed using Clampfit 10.3 software (Molecular Devices) and Igor Pro 6 software (Wavemetrics, Lake Oswego, OR) with the added import functionality provided by ReadPclamp XOP of the NeuroMatic software package (<http://www.neuromatic.thinkrandom.com/>). Representative current traces are shown after averaging four consecutive traces. To obtain inward current densities induced by MAM-2201 or WIN, the amplitudes of the current were normalized to membrane capacitances (picoamperes per picofarad, Fig. 2C). The densities were plotted as a function of the concentration and fit with the sigmoidal function, $Y = \text{Bottom} + (\text{Top} - \text{Bottom}) / (1 + [10]^{-(\text{LogEC50} - X) \cdot \text{Hillslope}})$, using GraphPad Prism 5 (GraphPad Software, San Diego, CA).

2.4. Cerebellar slice preparation and electrophysiological recordings from PCs

ICR mice of either sex [postnatal day (P) 20–57 for Figs. 3–5 and Table 1; P14–20 for Figs. 6 and 7, and Table 2] were used according to the guidelines for animal use of the National Institute of Health Sciences. Cerebellar slices were prepared as described previously with some modifications (Shuvaev et al., 2011). Briefly, mice were anesthetized with halothane and decapitated. Parasagittal slices of the cerebellum (200-μm thick) were prepared using a microslicer (PRO7, Dosaka, Kyoto, Japan) in ice-cold, cutting solution containing (in mM): 234 sucrose, 2.5 KCl, 1.25 NaH₂PO₄, 10 MgSO₄, 0.5 CaCl₂, 26 NaHCO₃, 11 glucose, and bubbled with 5% CO₂/95% O₂. The slices were then allowed to recover for 1 h at room temperature in artificial cerebrospinal fluid (ACSF) solution containing (in mM): 120 NaCl, 2.5 KCl, 2 CaCl₂, 1 MgCl₂, 1.25 NaH₂PO₄, 26 NaHCO₃, 17 glucose, 0.4 ascorbic acid, 3 myo-inositol, 2 sodium pyruvate, and bubbled with 5% CO₂/95% O₂. In electrophysiological recordings, ascorbic acid, myo-inositol, and sodium pyruvate were omitted.

Cerebellar slices were transferred to a recording chamber, and continuously perfused at 2 mL/min with ACSF at 25 ± 1 °C (Figs. 3–6 and Table 1) or near physiological temperature (34 ± 1 °C; Fig. 7 and Table 2). Electrophysiological recordings were done using the same equipment described above. Excitatory and inhibitory postsynaptic currents (EPSCs and IPSCs) were recorded in the presence of 100 μM picrotoxin (a GABA_A receptor antagonist, Tocris Bioscience) and 40 μM 6,7-dinitroquinoxaline-2,3-dione (DNQX, an AMPA/kainate receptor antagonist, Tocris Bioscience), respectively. Patch pipettes had a resistance of 2–3 MΩ when filled with pipette solutions. A CsCl-based and the K-gluconate-based internal solutions were used for voltage- (Figs. 3–6 and Table 1) and current-clamp recordings (Fig. 7 and Table 2), respectively. The CsCl-based solution contained (in mM): 120 CsCl, 20 K-gluconate, 15 tetraethylammonium-Cl, 3 MgCl₂, 5 EGTA, 5 Na₂-ATP, 5 Na₂-phosphocreatine, 0.3 Na₂-GTP, 5 QX-314, and 10 HEPES (pH adjusted to 7.3 with CsOH). The liquid junction potentials (CsCl-based, –4 mV; K-gluconate-based, –10 mV) were corrected off-line.

Somatic whole-cell patch-clamp recordings were performed from PCs in lobules IV to VIII. PF-PC EPSCs and IPSCs were evoked by electrical stimulation of the molecular layer and recorded at the holding potential of –80 mV. CF-PC EPSCs and complex spikes were evoked by the stimulation of the granule cell layer. CF-PC EPSCs were recorded at a holding potential of –10 mV to decrease the driving force for cations through ionotropic glutamate receptors. The stimuli (100- to 200-μs pulses, 20–80 V amplitude) were performed with an ACSF-filled patch pipette (tip diameter, 10–15 μm for molecular layer stimulation and 2–3 μm for the granule cell layer) and applied at 0.1 Hz. In some experiments, paired-pulse stimulation (50 ms inter-stimulus intervals) was done to calculate the paired-pulse ratio (PPR), which is an index of the change of neurotransmitter release from presynaptic terminals (Zucker and Regehr, 2002; Irie and

Ohmori, 2008). When postsynaptic currents were recorded, series resistance was monitored by applying small voltage steps (–10 mV, 20-ms duration), and the records were discarded if the resistance varied more than 25%. Quantal EPSCs (qEPSCs) from PFs and CFs were elicited by electrical stimulation (0.1 Hz) with PCs held at –80 mV and with CaCl₂ in ACSF replaced with equimolar SrCl₂ (Xu-Friedman and Regehr, 1999). Miniature IPSCs (mIPSCs) were recorded at a holding potential of –80 mV in the presence of 40 μM DNQX and 1 μM tetrodotoxin (TTX; Wako Pure Chemical Industries). In the start of current-clamp recordings, resting membrane potentials of PCs were adjusted at –60 to –70 mV by current injection to prevent spontaneous firing, and series resistance was compensated for using bridge balance and capacitance neutralization. Intrinsic membrane properties were examined by square-wave current injection (500-ms duration, Table 2). Input resistance was measured from averaged voltage responses evoked by small hyperpolarizing currents (–20 pA). Threshold current and threshold potential were measured by depolarizing current injections (from 0 pA to 200 pA, 20 pA increment). The maximum rate of rise and maximum rate of fall of action potentials and spike height were calculated from the first action potential waveform evoked at the threshold current. Firing frequency was obtained from the number of spikes observed during the current injection.

qEPSCs and mIPSCs were detected off-line using the template search function in the Clampfit 10.3 software. To analyze qEPSCs, data from 200 to 1600 ms after the stimulus artifact were used. Average cumulative probability histograms were obtained as follows: first, qEPSCs or mIPSCs were recorded more than 300 events from each cell in the presence or absence of MAM-2201. Then, for each cell, the amplitudes and inter-event intervals were binned, and individual cumulative probability histograms were plotted. Finally, these histograms were averaged. Representative EPSC and IPSC traces are shown after averaging four to six consecutive traces, and stimulus artifacts are truncated. EPSC and IPSC amplitudes were obtained by averaging six consecutive records. The coefficient of variation (CV), which is another index of the change of neurotransmitter release from presynaptic terminals, was calculated from 18 consecutive EPSC or IPSC traces (Korn and Faber, 1991). The inhibitory concentration 50% (IC50) values of the cannabinoid-related compounds against neurotransmitter release at PF-PC synapses were calculated as follows: control PF-PC EPSC amplitude was obtained from the averaged EPSCs recorded for 3 min before application of the synthetic cannabinoids. PF-PC EPSC amplitude in the presence of the cannabinoids was done from the EPSCs recorded for 8 to 10 min after the application, normalized to the control values, and plotted as a function of the concentration. The data were fit with the sigmoidal function, $Y = 100 / (1 + [10]^{(\text{LogIC50} - X) \cdot \text{Hillslope}})$ (Table 1). The reasons for using PF-PC synapses for measurement of IC50s were as follows: PF-PC synapses exhibit more stable synaptic transmission than interneuron-PC synapses (Vincent and Marty, 1996), they are more sensitive to CB1R agonists, and they express CB1R proteins more abundantly than CF-PC synapses (Kawamura et al., 2006).

2.5. Simultaneous recordings of Ca²⁺ transients and complex spikes

Current-clamp recordings were done from PCs using the K-gluconate-based intracellular solution in which EGTA was replaced with 100 μM Oregon Green 488 BAPTA-1 hexapotassium salt (OGB-1; Invitrogen, Carlsbad, CA) in the presence of picrotoxin. PC somata and dendrites were dialyzed with the pipette solution for 30 min to obtain a stable intracellular concentration of OGB-1. Confocal imaging was then performed with a Nipkow disk confocal scanner unit (CSU-10; Yokogawa Electric, Tokyo, Japan) attached to the Olympus BX51WI microscope with the 40× objective lens. A 488 nm beam from a diode laser (Yokogawa Electric) for excitation was coupled to the scanner unit through an optical fiber. Fluorescence was detected via a 520 nm long-path filter using an EMCCD camera (iXon3 DU897; Andor Technology, Belfast, Northern Ireland). The pixels were binned 2 × 2 on the chip, and images were acquired at 25.8 Hz. Complex spikes were evoked at 0.1 Hz, and the electrophysiological recordings were synchronized with the acquisition of time-lapse fluorescent images. The number of spikelets in complex spikes was obtained from average value of five to seven consecutive traces. The imaging experiments were controlled and analyzed using Andor iQ2 software (Andor Technology). Three to five consecutive time-lapse images were averaged and used for analysis. The regions of interests were set on primary dendrites (approximately between 20 and 100 μm from the center of the cell body, Fig. 7Ca). Fluorescence changes were background-corrected and expressed as ΔF/F₀, where F₀ is the fluorescence intensity when the cells were at rest, and ΔF is the absolute values of fluorescence changes during activity. Integration of Ca²⁺ transients was performed over 2 s from the onset.

All data other than EC50s or IC50s are provided as the means ± standard deviation. EC50s and IC50s are expressed as the best-fit values with 95% confidence interval (CI; Table 1). *n* indicates the number of experiments. Statistical significance was tested using paired *t*-tests test unless otherwise stated (significance, *p* < 0.05).

3. Results

3.1. MAM-2201 acts as an agonist of hCB1Rs and mCB1Rs

To examine whether MAM-2201 activates CB1Rs, we expressed hCB1R or mCB1R cDNAs in murine tumor line AtT-20. Because

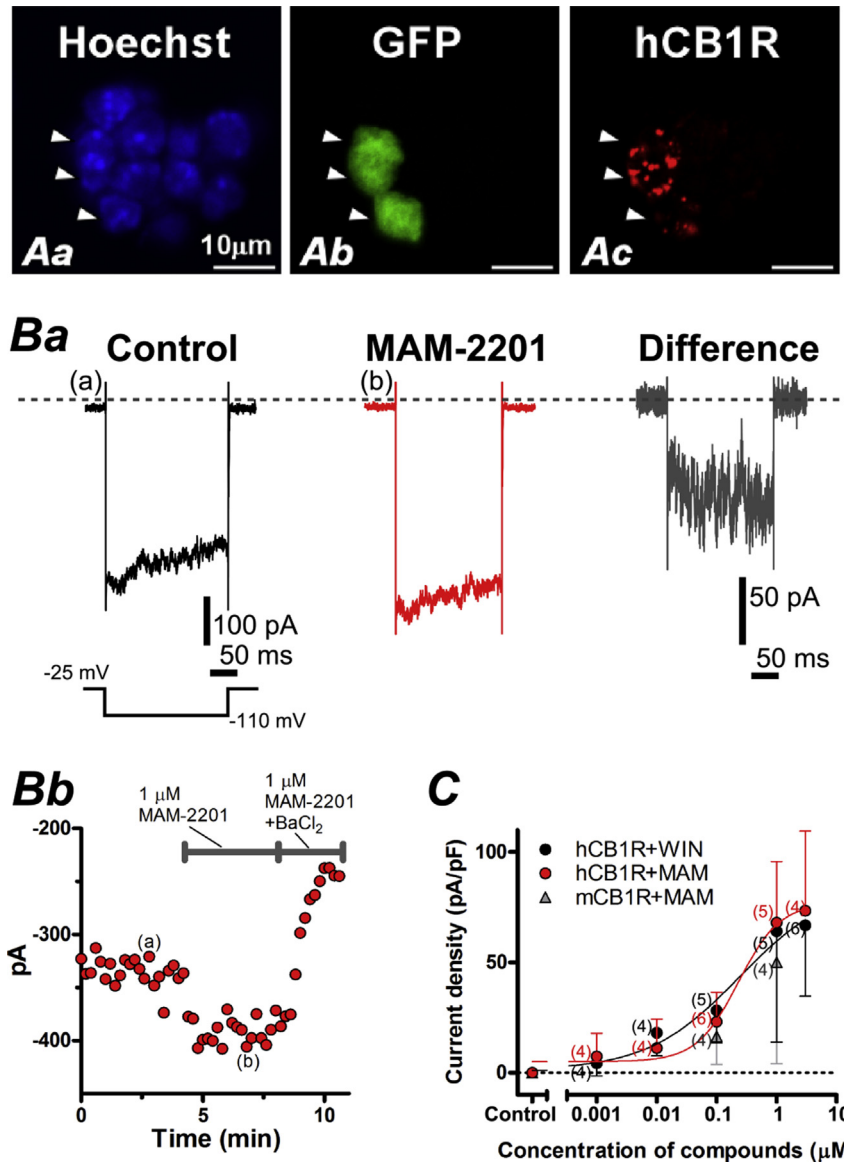


Fig. 2. Heterologous expression of cannabinoid receptor type 1 (CB1R) cDNAs in AtT-20 cells. A, Immunofluorescence images of AtT-20 cells transfected with human CB1R (hCB1R) and green fluorescent protein (GFP) cDNAs. Cell nuclei were stained with Hoechst 33342 (1 μg/mL, Dojindo, Kumamoto, Japan; Aa). Arrowheads indicate GFP and hCB1R double positive cells. Proteins of hCB1Rs were visualized by immunolabelling with rabbit anti-CB1R antibody and AlexaFluor 568-conjugated anti-rabbit secondary antibody (Ac). B, Representative data recorded from hCB1R-expressing cell. Ba, Inward currents were evoked by applying voltage steps from a holding potential of -25 mV to -110 mV for 200 ms. In trace (a) and (b), averages of four consecutive responses are shown. These traces correspond to the responses at time points marked (a) or (b) in Bb. The holding current level is shown by a dotted line. Bb, Time course of mean inward currents. Each point represents an averaged value obtained from four consecutive records. C, Concentration-dependent increases of inward current densities induced by MAM-2201 or (R)-(+)-[2,3-Dihydro-5-methyl-3-(4-morpholinylmethyl)pyrrolo[1,2,3-de]-1,4-benzoxazin-6-yl]-1-naphthalenylmethanone mesylate [WIN55,212-2 (WIN)]. To obtain current densities, amplitudes of inward current induced by MAM-2201 or WIN, were normalized to membrane capacitances (picoamperes per picofarad). The densities were plotted as a function of the concentration and fit with the sigmoidal function, $Y = \text{Bottom} + (\text{Top} - \text{Bottom}) / (1 + 10^{-(\text{LogEC}_{50} - X) \cdot \text{Hillslope}})$, where EC₅₀ is effective concentration 50%. Here and in the following figures, error bars and the numbers in parentheses indicate standard deviation and the number of experiments, respectively.

application of CB1 agonists on AtT-20 cells expressing CB1Rs activates inward rectifier potassium currents, activities of compounds against CB1Rs can be determined using this heterologous expression system (Mackie et al., 1995; Felder et al., 1998). Whole-cell patch clamp recordings were done from hCB1R or mCB1R-expressing cells, and inward currents were evoked by applying hyperpolarizing voltage pulses (Fig. 2B). Bath application of MAM-2201 (1 μM) increased the amplitude of inward current within 5 min (Fig. 2Bb). Subsequent application of low concentration of Ba²⁺ (200 μM BaCl₂), which blocks inward rectifier potassium

currents (Hagiwara et al., 1976), markedly reduced the inward currents. This indicates that, in addition to MAM-2201-induced currents, MAM-2201-independent inward rectifier potassium currents were simultaneously blocked (Dousmanis and Pennefather, 1992). The time course of the induced current, obtained by subtracting the currents before from those after the application of MAM-2201, showed slow activation at the beginning of voltage pulse (Fig. 2Ba, Difference). This property is characteristic of activation of G-protein coupled potassium channels (Kubo et al., 1993). Fig. 2C shows the concentration-dependent increase of current

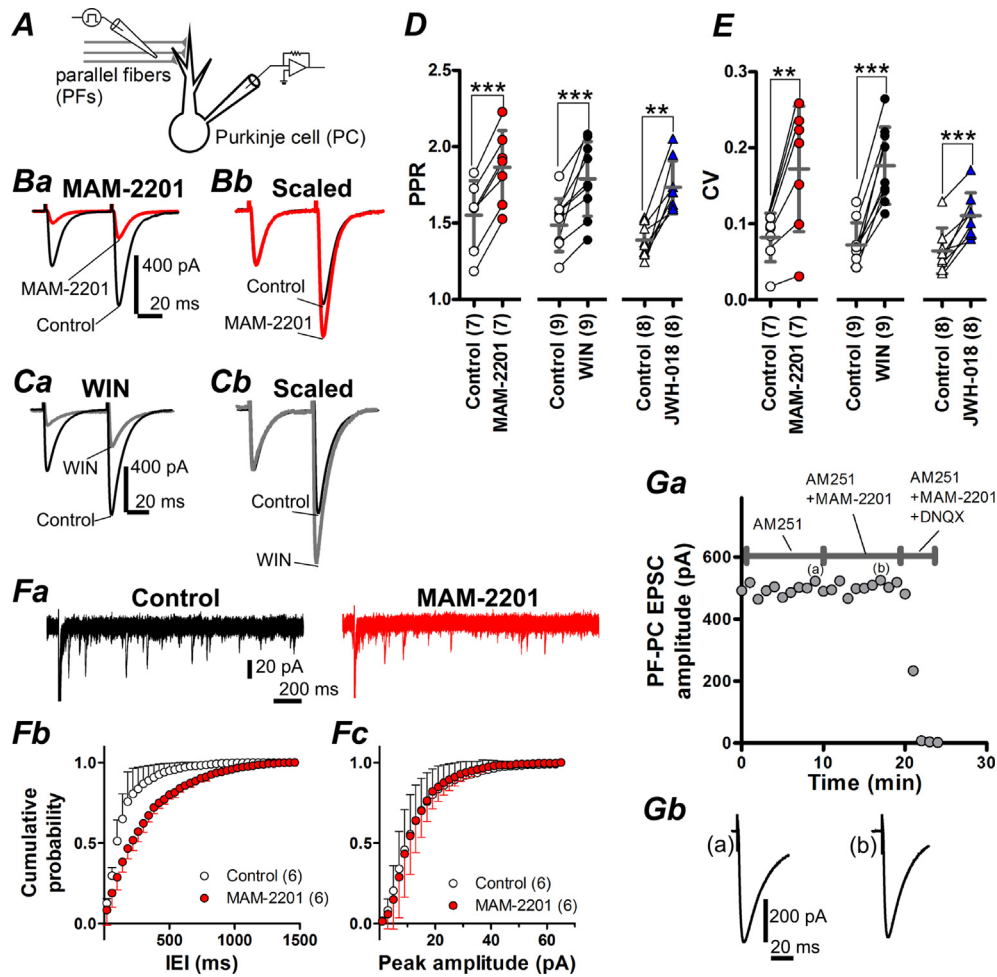


Fig. 3. MAM-2201 inhibits synaptic transmission at parallel fiber (PF)-Purkinje cell (PC) synapses presynaptically via activation of presynaptic CB1Rs. **A**, Experimental configuration for Fig. 3B–G and 4. **B**, PF-induced excitatory postsynaptic currents (EPSCs) were evoked with pairs of stimuli (50 ms interval) under control conditions (Control) or in the presence of 10 μM MAM-2201 (MAM-2201). The holding potential was -80 mV. Picrotoxin (100 μM) was added to the extracellular artificial cerebrospinal fluid (ACSF) to block GABA_A receptor-mediated inhibitory postsynaptic currents (IPSCs). The first EPSC peak in MAM-2201 was reduced to 21.9% of control. In each trace, averages of six trials are shown. In the right panel, the EPSC evoked by the first stimulus in MAM-2201 is scaled to the amplitude of the first EPSC in Control. MAM-2201 increased paired-pulse facilitation (**Bb**). Stimulus artifacts are truncated. **C**, Same as in **A**, but in the presence of 10 μM WIN. In **Ca**, the first peak in WIN was reduced to 24.1% of control. In the right panel, the EPSC evoked by the first stimulus in WIN is scaled to the amplitude of the first EPSC in Control. **D** and **E**, Summary of paired-pulse ratio (PPR, **D**) and coefficient of variation (CV, **E**) of PF-PC EPSCs before and after application of MAM-2201, WIN, or JWH-018 (10 μM in all groups). Here and in the following figures, the statistical significance was tested using paired *t*-tests unless otherwise stated (significance, $p < 0.05$). $**p < 0.01$ and $***p < 0.001$. **F**, To isolate quantal EPSCs (qEPSCs) from PFs, asynchronous neurotransmitter release from PF terminals was evoked by stimulating PFs in the presence of Sr^{2+} (2 mM, see Materials and Methods). **Fa**, Five superimposed traces before (Control) and after application of MAM-2201. Asynchronously released quanta are seen as downward current deflections. Synchronous PF-PC EPSCs are truncated. **Fb** and **Fc**, Average cumulative probability histograms of inter-event interval (IEI, **Fb**, bin width: 40 ms) and peak amplitude (**Fc**, bin width: 2 pA) of PF-PC qEPSCs. **Ga**, Time course of peak PF-PC EPSC amplitudes in the presence of *N*-(Piperidin-1-yl)-5-(4-iodophenyl)-1-(2,4-dichlorophenyl)-4-methyl-1*H*-pyrazole-3-carboxamide (AM251, 5 μM). Each point represents an averaged value obtained from six consecutive records. MAM-2201 (10 μM) had no detectable effect on the amplitude. Additional application of 6,7-dinitroquinoxaline-2,3-dione (DNQX, 40 μM) abolished PF-PC EPSCs completely. **Gb**, Traces show normalized PF-PC EPSC responses at time points marked (a) and (b) in **Ga**.

densities induced by MAM-2201 or WIN in CB1R-expressing cells. Interestingly, in hCB1R-expressing cells, MAM-2201 increased current densities in a concentration-dependent manner (Fig. 2C, red circles) with an EC₅₀ of 0.230 μM (95% CI, 0.0384–1.37 μM). Similar responses were obtained by application of WIN (Fig. 2C, black circles; EC₅₀ = 0.234 μM ; 95% CI, 0.410×10^{-3} –140 μM), which was consistent with previous report (Mackie et al., 1995). In the presence of AM251 (5 μM , a CB1R antagonist), MAM-2201 (1 μM) did not induce the inward currents (-2.38 ± 7.23 pA/pF, $n = 6$). In cells transfected with GFP alone, MAM-2201 (1 μM) did not elicit any changes (1.55 ± 6.78 pA/pF, $n = 5$). In mCB1R-expressing cells, MAM-2201 induced concentration-dependent increase in the current density (Fig. 2C, gray triangles). These results demonstrate that MAM-2201 activates hCB1Rs and mCB1Rs.

3.2. MAM-2201 inhibits synaptic transmission presynaptically via activation of presynaptic CB1Rs at PF-PC synapses in mouse cerebellum

We tested the effects of MAM-2201 on neurotransmitter release at PF-PC synapses and the involvement of CB1Rs (Fig. 3), and compared the potency of MAM-2201 with that of WIN, JWH-018, and Δ^9 -THC (Fig. 4 and Table 1). Whole-cell patch-clamp recordings were performed from somata of PCs in mouse cerebellar slices under voltage-clamp conditions, and PF-PC EPSCs were evoked by electrical stimulation of PFs in the molecular layer in the presence of picrotoxin. The recording configuration is illustrated in Fig. 3A. As shown in Fig. 3B, bath application of MAM-2201 (10 μM , 8 min) significantly decreased the first EPSC amplitude

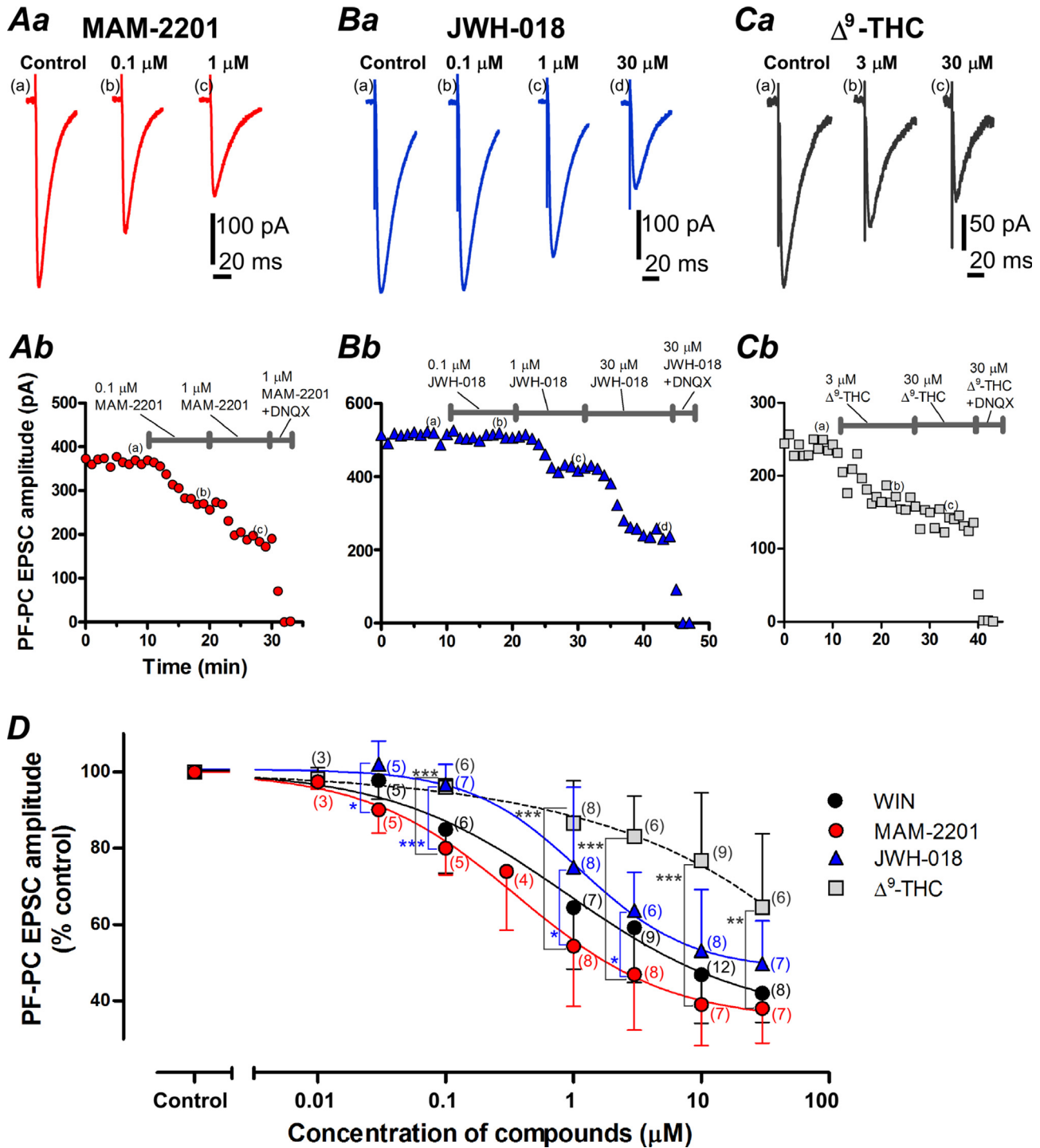


Fig. 4. MAM-2201 is a more potent inhibitor than Δ^9 -tetrahydrocannabinol (Δ^9 -THC) and JWH-018 at PF-PC synapses. **Aa**, Representative PF-PC EPSC traces recorded in control conditions, or in 0.1 or 1 μ M MAM-2201. These traces show normalized PF-PC EPSC responses at time points marked (a), (b), or (c) in **Ab**. **Ab**, Time course of peak amplitudes of PF-PC EPSCs. Each point represents an averaged value obtained from six consecutive records. **Ba**, Representative PF-PC EPSC traces recorded in control conditions, or in 0.1, 1, or 30 μ M JWH-018. These traces correspond to the responses at time points marked (a), (b), (c), or (d) in **Bb**. **Bb**, Time course of peak amplitudes of PF-PC EPSCs. **C**, Representative PF-PC EPSC traces recorded in control conditions, or in 3, or 30 μ M Δ^9 -THC. These traces correspond to the responses at time points marked (a), (b), or (c) in **Cb**. **Cb**, Time course of the peak amplitudes. In **Aa**, **Ba**, and **Ca**, stimulus artifacts are truncated. **D**, Concentration-dependent decreases of PF-PC EPSC amplitudes induced by cannabinoid-related compounds. Control PF-PC EPSC amplitude was obtained from averaged PF-PC EPSCs recorded for 3 min before the application of the compounds. PF-PC EPSC amplitudes in the presence of these compounds were recorded for 8–10 min after application, normalized to the control values, and plotted as a function of concentration (Fig. 4C). Each plot was fit with a sigmoidal function, $Y = 100 / (1 + [10]^{(LogIC50 - X) \cdot Hillslope})$, where IC50 is inhibitory concentration 50%. * $p < 0.05$, ** $p < 0.01$, and *** $p < 0.001$ by unpaired t -tests test.

(39.0 \pm 10.8% of control value, $n = 7$, $p < 0.001$). To investigate whether the effects of MAM-2201 on PF-PC EPSC amplitude were mediated by presynaptic mechanisms, PPR and CV analyses were performed. MAM-2201 (10 μ M) significantly increased PPR

(Fig. 3Bb and D) and CV (Fig. 3E), indicating a decrease in presynaptic neurotransmitter release. WIN (10 μ M, 8-min application) induced a similar decrease in PF-PC EPSC amplitude and a parallel increase in the PPR and CV (Fig. 3C–E). MAM-2201 (10 μ M) also

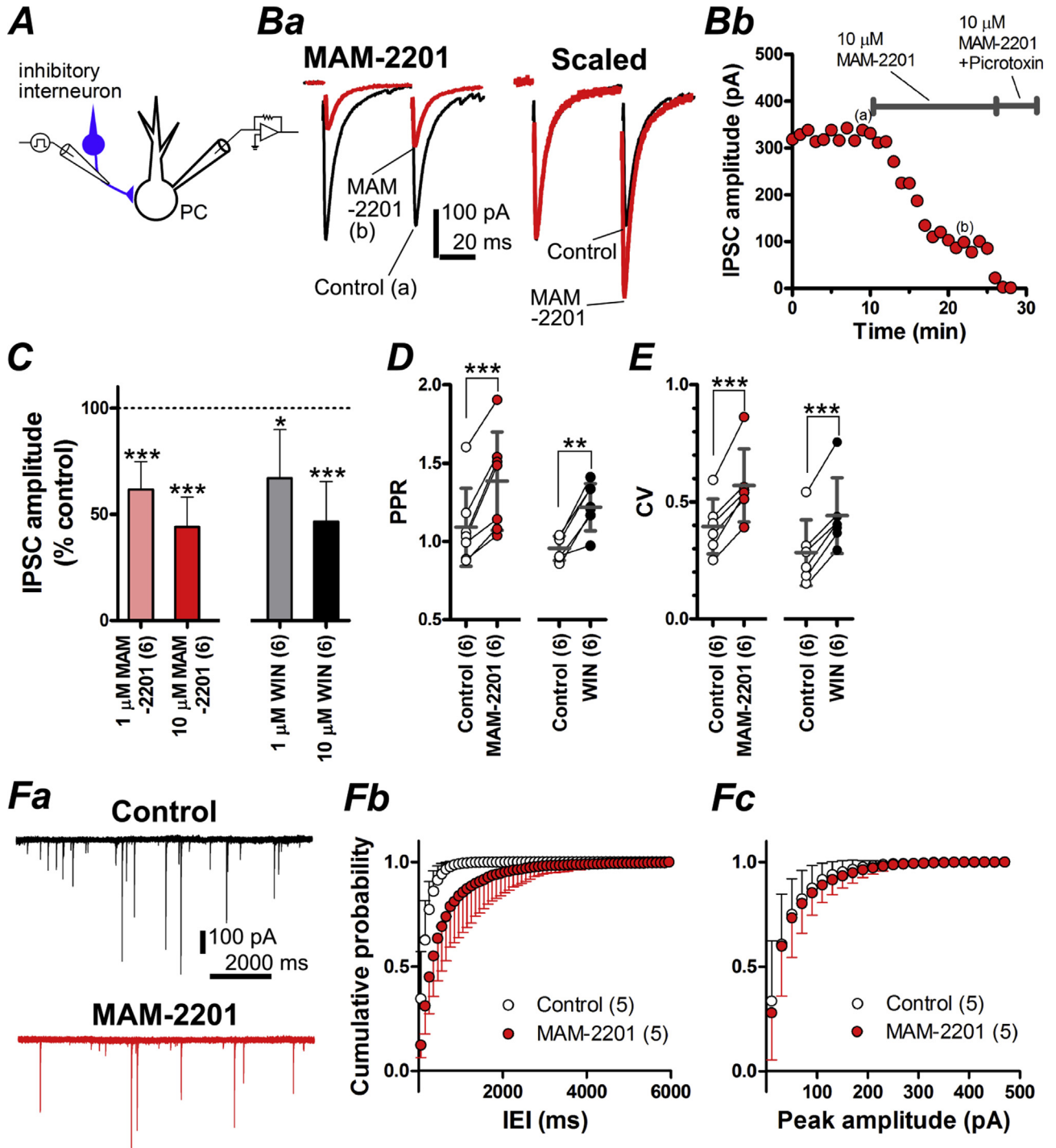


Fig. 5. MAM-2201 reduces GABAergic synaptic transmission at interneuron-PC synapses via presynaptic mechanisms. **A**, Experimental configuration for Fig. 5B–E. **Ba**, Averaged current traces of IPSCs in control conditions (Control) and 10 μ M MAM-2201. These traces show normalized IPSC responses at time points marked (a) and (b) in **Bb**. IPSCs were evoked with pairs of stimuli (50 ms interval) in the presence of 40 μ M DNQX and were recorded as inward currents because of the use of the CsCl-based internal solution. The holding potential was -80 mV, and stimulus artifacts were blanked for clarity. The first peak in MAM-2201 was reduced to 28.0% of control. In the right panel, the first IPSC in MAM-2201 is scaled to the amplitude of the first IPSC in Control (Scaled), showing a clear increase of PPR. **Bb**, Time course of peak amplitudes of the first IPSC. Each point represents an averaged value obtained from six consecutive records. **C**, Concentration-dependent decreases of peak amplitude of IPSC by MAM-2201 and WIN. IPSC amplitudes were normalized to the control value (=baseline responses) and expressed as a percentage of control. $*p < 0.05$ and $***p < 0.001$. **D** and **E**, Summary of PPR (**D**) and CV (**E**) of IPSCs before and after application of MAM-2201 and WIN (10 μ M in both groups). $**p < 0.01$. **F**, Miniature IPSCs (mIPSCs) recorded in the presence of tetrodotoxin (TTX, 1 μ M) and DNQX. **Fa**, Five superimposed traces before (Control) and after application of MAM-2201. mIPSCs appear as downward current deflections. **Fb** and **Fc**, Average cumulative probability histograms of IEI (**Fb**, bin width: 100 ms) and peak amplitude (**Fc**, bin width: 20 pA) of mIPSCs.

decreased PF-PC qEPSC frequency [Inter-event interval (IEI), Control: 194.0 ± 24.1 ms, MAM-2201: 288.7 ± 30.2 ms, $p < 0.001$, $n = 6$, Fig. 3Fa and Fb] without affecting PF-PC qEPSC amplitude (peak amplitude, Control: 18.9 ± 2.1 pA, MAM-2201: 18.6 ± 4.3 pA,

$p = 0.860$, $n = 6$, Fig. 3Fa and Fc). In the absence of MAM-2201, amplitudes of PF-PC EPSCs did not show significant changes during 45-min recording under condition in which series resistance was stable ($105.2 \pm 10.5\%$ of control, $n = 7$, $p = 0.271$).

Table 1
IC50s of synthetic cannabinoids against PF-PC EPSCs.

	WIN	MAM-2201	JWH-018
IC50 (μM)	0.890 [0.296–2.679]	0.363 [0.193–0.681]	1.121 [0.551–2.282]
[95% CI (μM)] ^a			
Relative IC50	1.00	0.41	1.25

^a Data are provided as the best-fit values with 95% confidence intervals (CI).

To examine whether MAM-2201 altered postsynaptic responses by activating presynaptic CB1Rs, MAM-2201 was bath-applied to the cerebellar slices in the presence of AM251 (5 μM). MAM-2201 did not induce any change of PF-PC EPSC amplitude in the presence of AM251 (Fig. 3G, $102.2 \pm 6.0\%$ of control, $n = 5$, $p = 0.443$).

Subsequent application of DNQX (40 μM) abolished PF-PC EPSCs, demonstrating that glutamatergic synaptic transmission was indeed evoked, and bath application of these chemicals was successful (Fig. 3Ga). Taken together, these results indicate that the MAM-2201-induced changes are mediated by a decrease in presynaptic neurotransmitter release from PF terminals via activation of presynaptic CB1Rs.

3.3. MAM-2201 is a more potent inhibitor of PF-PC synapses than Δ^9 -THC and JWH-018

Fig. 4A–C show representative traces of PF-PC EPSCs in the presence of MAM-2201 (Fig. 4A), JWH-018 (Fig. 4B), or Δ^9 -THC (Fig. 4C), respectively. The inhibitory effect of MAM-2201 on PF-PC

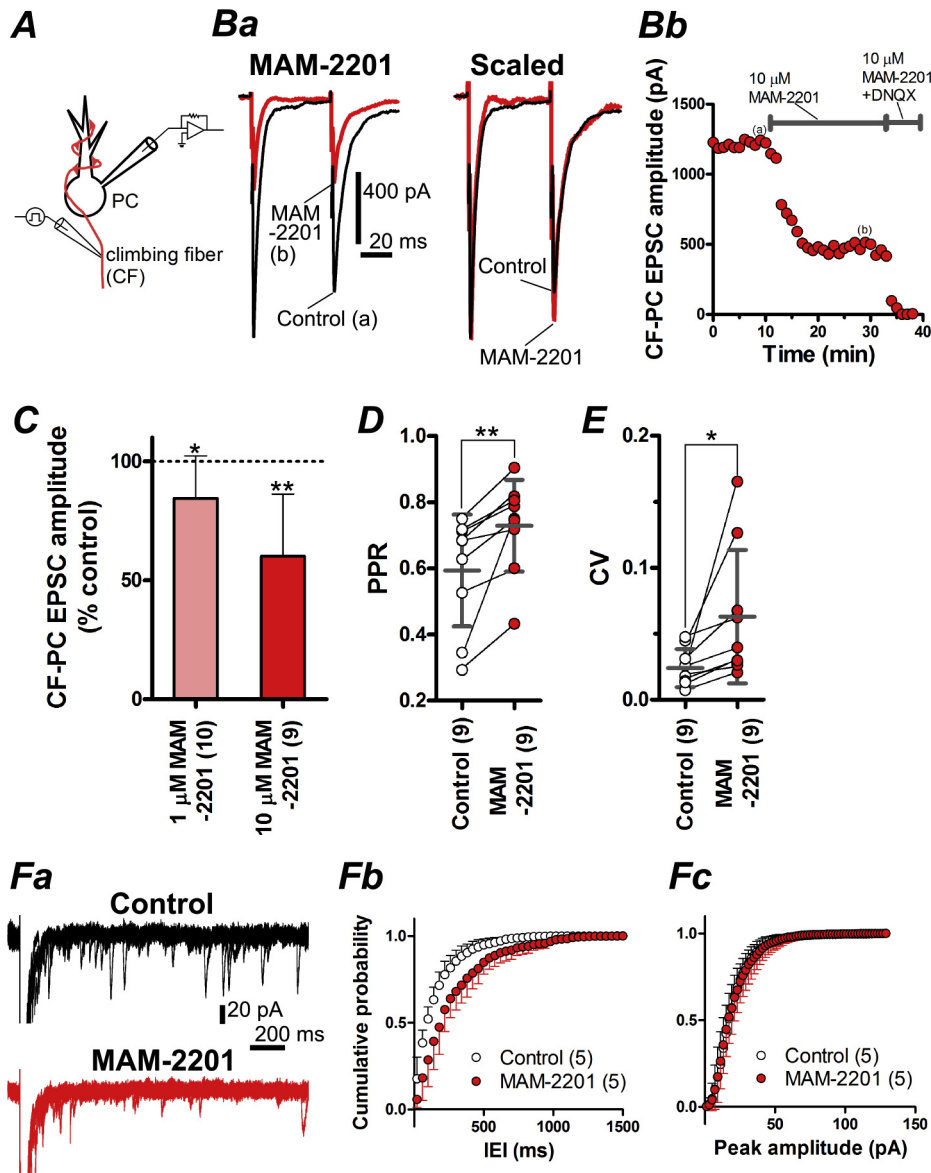


Fig. 6. MAM-2201-mediated presynaptic inhibition at climbing fiber (CF)-PC synapses. **A**, Experimental configuration for Fig. 6B–F and 7. **Ba**, Averaged current traces of CF-PC EPSCs in control (Control) and 10 μM MAM-2201. These traces show normalized CF-PC EPSC responses at time points marked (a) and (b) in **Bb**. CF-PC EPSCs were evoked with pairs of stimuli (50 ms interval) in the presence of 100 μM picrotoxin. PCs were held at -10 mV to reduce the driving force for AMPA receptor-mediated currents. Stimulus artifacts were truncated for clarity. The first peak in MAM-2201 was reduced to 38.4% of control. In the right panel, the first CF-PC EPSC in MAM-2201 is scaled to the amplitude of the first CF-PC EPSC of control (Scaled). **Bb**, Time course of peak amplitudes of first CF-PC EPSC. Each point represents an averaged value obtained from six consecutive records. **C**, Concentration-dependent decreases of the peak amplitudes of CF-PC EPSCs by MAM-2201. CF-PC EPSC amplitudes were expressed as a percentage of control. * $p < 0.05$ and ** $p < 0.001$. **D** and **E**, Summary of PPR (**D**) and CV (**E**) of CF-PC EPSCs before and after application of MAM-2201 (10 μM). **F**, CF-PC qEPSCs in the presence of picrotoxin and Sr^{2+} (2 mM SrCl_2). The qEPSCs were recorded at a holding potential of -80 mV. **Fa**, Five superimposed traces before (Control) and after application of MAM-2201. Synchronous CF-PC EPSCs are truncated. **Fb** and **Fc**, Average cumulative probability histograms of IEI (**Fb**, bin width: 40 ms) and peak amplitude (**Fc**, bin width: 2 pA) of CF-PC qEPSCs.

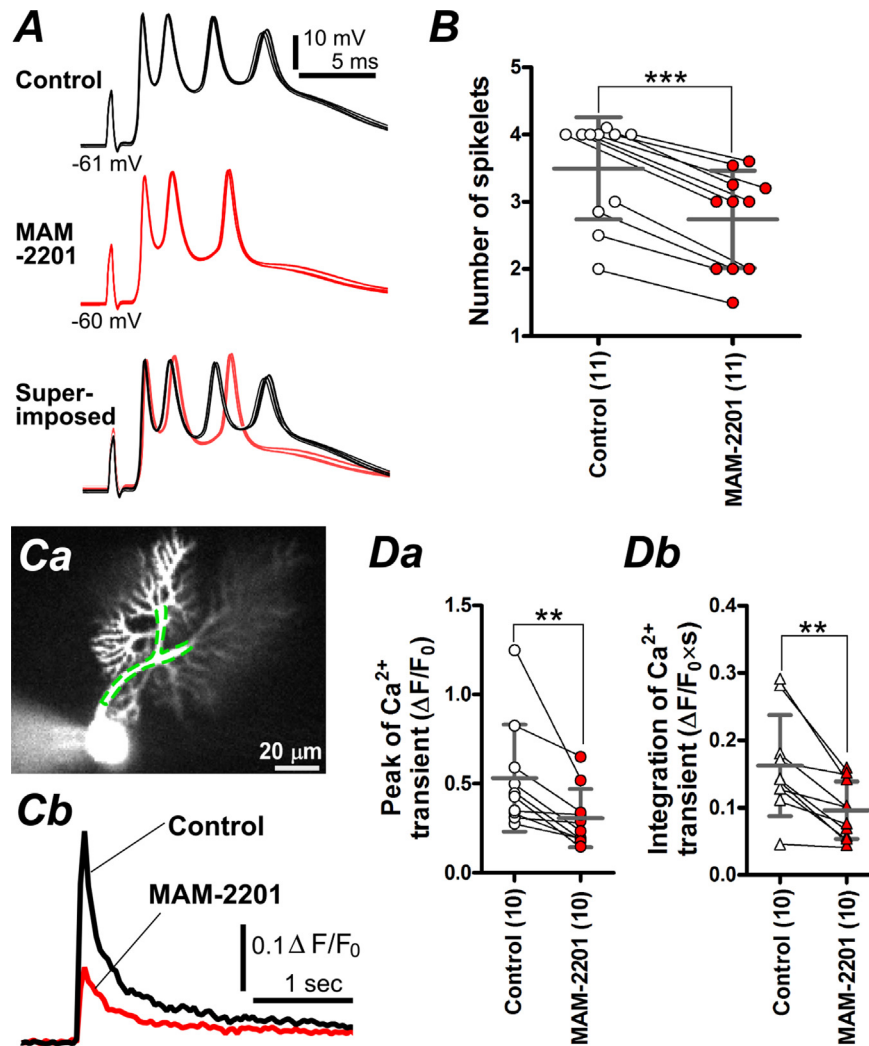


Fig. 7. MAM-2201 reduces the number of spikelets in complex spikes and dendritic Ca^{2+} transients evoked by CF stimulation. **A–D**, Simultaneous recordings of complex spikes and dendritic Ca^{2+} transients. **A**, Representative superimposed traces of complex spikes (5 traces) evoked by stimulation of CFs (0.1 Hz) in the presence of picrotoxin at near physiological temperature ($34 \pm 1^\circ C$). The K-gluconate-based intracellular solution containing Oregon Green 488 BAPTA-1 hexapotassium salt (OGB-1, 100 μ M) was used for current-clamp recordings. At the start of the recording, the resting membrane potential was adjusted around -60 to -70 mV by current injection to prevent spontaneous firing. MAM-2201 (10 μ M, 10 min) reduced the number of spikelets (4 spikelets in Control; 3 spikelets in MAM-2201). Superimposed traces reveal delay and reduction of spikelets in MAM-2201. **B**, Summary of average number of spikelets before and after application of MAM-2201 (10 μ M). *** $p < 0.001$. **C**, A dendritic Ca^{2+} transient induced by CF stimulation. Intracellular Ca^{2+} measurement in **C** was simultaneously performed while recording the complex spikes in **A**. **Ca**, Representative confocal image of PC loaded with OGB-1 via a patch pipette. Area indicated by dotted line represents region of interest used for the calculation of the dendritic Ca^{2+} transients. **Cb**, Representative Ca^{2+} transients in control and MAM-2201 (10 μ M). F_0 is the fluorescence intensity when the cells were at rest, and ΔF is the absolute values of fluorescence changes during activity. **Da** and **Db**, Summary of Ca^{2+} transient peaks (**Da**) and integration of Ca^{2+} transients (**Db**). The integration was performed for 2 s from the onset. ** $p < 0.01$.

EPSC amplitude was first detectable at 0.03 μ M (Fig. 4D, $90.1 \pm 6.1\%$ of control, $n = 5$, $p < 0.05$), and became more apparent at higher concentrations. Application of 0.1 μ M MAM-2201 was sufficient to induce a clear reduction [trace (b) in Fig. 4Aa, 71.9% of control], and subsequent administration of 1 μ M MAM-2201 induced further decrease [trace (c) in Fig. 4Aa, 51.0% of control]. On the other hand, 0.1 μ M JWH-018 did not have detectable effects on PF-PC EPSCs [trace (b) in Fig. 4Ba, 99.0% of control; 0.1 μ M JWH-018 in Fig. 4D, $n = 7$, $p = 0.096$]. Higher concentrations of JWH-018 were required to reduce PF-PC EPSC amplitude [trace (c) in Fig. 4Ba, 1 μ M, 81.0% of control; trace (d) in Fig. 4Ba, 30 μ M, 44.2% of control]. Application of Δ^9 -THC, which acts as a partial agonist of CB1Rs (Shen and Thayer, 1999; Luk et al., 2004), decreased amplitude of PF-EPSCs obviously at 3 μ M [trace (b) in Fig. 4C, 68.6% of control], but subsequent administration of 30 μ M Δ^9 -THC did not induce a clear reduction [trace (c) in Fig. 4C, 57.0% of control]. Δ^9 -THC (30 μ M) significantly

increased PPR and CV ($n = 6$, data not shown), indicating a decrease in presynaptic neurotransmitter release. Fig. 4D shows the concentration-dependent decreases of PF-PC EPSC amplitude induced by cannabinoid-related compounds. MAM-2201 decreased PF-PC EPSCs more potently than JWH-018 within the range of 0.03–3 μ M (Fig. 4D, blue triangles (in the web version), $p < 0.05$ and $p < 0.01$ by unpaired t -tests test) and Δ^9 -THC within the range of 0.1–30 μ M (Fig. 4D, gray squares, $p < 0.001$ by unpaired t -tests test). Application of WIN decreased PF-PC EPSC amplitude to $64.5 \pm 0.16\%$ ($n = 7$) of the control value at a concentration of 1 μ M and to $46.8 \pm 0.13\%$ ($n = 12$) at 10 μ M (Fig. 4D, WIN). These results are comparable to the previous reports using cerebellar slice preparations from rodents (see Discussion) (Levenes et al., 1998; Takahashi and Linden, 2000; Kawamura et al., 2006). The IC₅₀s of the synthetic cannabinoids against PF-PC EPSCs are summarized in Table 1, and indicate that the rank order of potency for inhibition is MAM-

Table 2
MAM-2201 did not affect intrinsic membrane properties of PCs.

	Control (n = 10)	10 μ M MAM-2201 (n = 10)	p value
Resting membrane potential (mV)	-65.3 ± 3.2	-66.0 ± 3.5	0.43
input resistance (M Ω)	113 ± 51	101 ± 34	0.29
Threshold current (pA)	71.0 ± 39.5	77.8 ± 7.4	0.24
Threshold potential (mV)	-45.4 ± 5.6	-44.9 ± 6.4	0.50
Spike height (mV)	44.9 ± 6.4	45.4 ± 47.6	0.71
Maximum rate of rise (V/s)	114 ± 40	131 ± 37	0.20
Maximum rate of fall (V/s)	-93.0 ± 17	-89.2 ± 15.8	0.14
Firing frequency at 200 pA (Hz)	33.0 ± 18.4	34.4 ± 20.5	0.77
Firing frequency at 500 pA (Hz)	72.6 ± 29.8	77.8 ± 42.1	0.68

Young mice (P14–20) and the K-gluconate-based internal solution were used for the experiments. Current-clamp recordings were performed at near physiological temperature ($34 \pm 1^\circ\text{C}$).

Data are provided as the means \pm standard deviation, and n = number of experiments.

2201 > WIN > JWH-018. These findings are consistent with our unpublished data on the IC50s for these synthetic cannabinoids, measured by a binding assay for human recombinant CB1Rs (see Discussion). IC50 of Δ^9 -THC was not able to be calculated due to ambiguous fitting. These results demonstrate that MAM-2201 is a more potent inhibitor of PF-PC synaptic transmission than JWH-018 and Δ^9 -THC.

3.4. MAM-2201 inhibits GABAergic synaptic transmission at inhibitory interneuron-PC synapses via presynaptic mechanisms

PCs receive feed-forward inhibition from GABAergic inhibitory interneurons lying in the molecular layer of the cerebellar cortex (Llinas et al., 2004), and this inhibition shapes the spike output of PCs (Mittmann et al., 2005). To explore how MAM-2201 modulates this inhibitory synaptic input, we recorded GABAergic synaptic transmission at inhibitory interneuron-PC synapses and examined the effects of MAM-2201 on inhibitory transmission. As shown in Fig. 5B, 10 μ M MAM-2201 decreased the first IPSC amplitude (MAM-2201 in Fig. 5Ba and Bb; Fig. 5C, $n = 6$, $p < 0.001$), and a similar reduction was observed by 1 μ M MAM-2201, indicating the MAM-2201-induced decrease was concentration-dependent (Fig. 5C, MAM-2201). MAM-2201 (10 μ M) significantly increased PPR and CV (Scaled in Fig. 5Ba, D and E, MAM-2201), and these increases were comparable to those obtained by WIN (10 μ M, Fig. 5D and E, WIN). Moreover, MAM-2201 (10 μ M) decreased mIPSC frequency (IEI, Control: 451.2 ± 464.1 ms, MAM-2201: 718.8 ± 542.9 ms, $p < 0.05$, $n = 5$, Fig. 5Fa and Fb) without affecting mIPSC amplitude (peak amplitude, Control: 45.3 ± 22.3 pA, MAM-2201: 48.3 ± 24.1 pA, $p = 0.53$, $n = 5$, Fig. 5Fa and Fc). These results demonstrate that MAM-2201 inhibits GABAergic synaptic transmission at interneuron-PC synapses via presynaptic mechanisms.

3.5. MAM-2201-mediated presynaptic inhibition at CF-PC synapses reduces the number of spikelets in complex spikes and dendritic Ca^{2+} transients in PCs

Activation of CFs produces AMPA receptor-mediated strong postsynaptic depolarization and evokes an all-or-none spike with multiple peaks (spikelets), called “complex spikes” in the soma (Llinas et al., 2004). Complex spikes are accompanied by a large, dendritic Ca^{2+} transient, which plays a crucial role in producing long-term depression (LTD) at PF-PC synapses (Konnerth et al., 1992). At CF terminals, activation of presynaptic CB1Rs by WIN reduces glutamate release (Maejima et al., 2001). To examine how presynaptic modulation by MAM-2201 at CF-PC synapses affects

the waveforms of complex spikes and CF-induced dendritic Ca^{2+} transients, we first confirmed presynaptic inhibition by MAM-2201 at CF-PC synapses (Fig. 6), and then performed simultaneous recordings of complex spikes and intracellular Ca^{2+} transients (Fig. 7).

First, CF-PC EPSCs were recorded at the holding potential of -10 mV in the presence of picrotoxin (Fig. 6B–E). To improve the space clamp in dendrites, young mice (P14–20) were used for the following experiments. This was because CF innervation of PCs is almost matured at this age (Hashimoto and Kano, 2013), and their dendrites are compact compared with those of adult (\sim P57) mice (McKay and Turner, 2005). As shown in Fig. 6B and C, bath application of MAM-2201 (1 or 10 μ M) reduced CF-PC EPSC amplitude in a concentration-dependent manner. This reduction was accompanied by significant increases in PPR and CV (10 μ M MAM-2201; Scaled in Fig. 6Ba, C and D). Moreover, MAM-2201 (10 μ M) decreased CF-PC qEPSC frequency (IEI, Control: 176.5 ± 40.3 ms, MAM-2201: 234.5 ± 51.1 ms, $p < 0.01$, $n = 5$, Fig. 6Fa and Fb) without affecting CF-PC qEPSC amplitude (peak amplitude, Control: 22.5 ± 2.7 pA, MAM-2201: 22.0 ± 4.0 pA, $p = 0.75$, $n = 5$, Fig. 6Fa and Fc). These results indicate that MAM-2201 presynaptically inhibits neurotransmitter release from CF terminals.

We then simultaneously recorded complex spikes in the somata and Ca^{2+} transients in the dendrites of PCs using the K-gluconate-based internal solution containing OGB-1 at near physiological temperature. Complex spikes were elicited under current-clamp conditions. As presented in Fig. 7A, electrical stimulation of CFs evoked all-or-none complex spikes consisting of spikelets (Control in Fig. 7A). MAM-2201 (10 μ M, 10 min) significantly reduced the number of spikelets to 78% of the control (Fig. 7B, $n = 11$, $p < 0.001$). Because MAM-2201 modulated synaptic properties via activation of presynaptic CB1Rs (Fig. 3), and because PCs do not express CB1Rs (Kano et al., 2009), we would not expect MAM-2201 to affect the intrinsic membrane properties of PCs. As expected, we were able to confirm that MAM-2201 did not affect the resting membrane potential, input resistance, or action potential properties of PCs (Table 2). Accordingly, MAM-2201-induced changes in complex spike waveforms can be interpreted based on depression of CF-PC EPSCs. The complex spikes evoked by CF stimulation were accompanied by large Ca^{2+} transients in the dendrites (Fig. 7Cb, Control). MAM-2201 substantially decreased the peak amplitude of the Ca^{2+} transient (Fig. 7Cb, MAM-2201). Both the peak and the integral of the Ca^{2+} transients were significantly attenuated by 10 μ M MAM-2201 (peak: $n = 10$, $p < 0.01$, Fig. 7Da; integration: $n = 10$, $p < 0.01$, Fig. 7Db). Taken together, these results indicate that MAM-2201 alters PC responses to CF activation by reducing the number of spikelets and the dendritic Ca^{2+} transients. This implies that MAM-2201 would decrease complex spike-mediated information propagation from PCs to the next nuclei and might affect induction of intracellular Ca^{2+} -dependent LTD at PF-PC synapses (see Discussion).

4. Discussion

This is the first study of the effects of MAM-2201 on neuronal functions. We found that MAM-2201 acted as an agonist of CB1Rs (Fig. 2). We also found that MAM-2201 inhibited glutamatergic synaptic transmission presynaptically via activation of presynaptic CB1Rs (Fig. 3). At the same concentrations, MAM-2201 decreased PF-PC EPSCs more potently than JWH-018 and Δ^9 -THC (Fig. 4). Moreover, MAM-2201 also presynaptically suppressed GABAergic synaptic transmission at interneuron-PC synapses (Fig. 5) and glutamatergic synaptic transmission at CF-PC synapses (Fig. 6). In the case of smaller CF-PC EPSCs, MAM-2201 led to reduction of the number of action potentials in complex spikes and to reduced

dendritic intracellular Ca^{2+} transients (Fig. 7). Thus, it is likely that, in humans, the psychoactive effects caused by MAM-2201 are mainly due to inhibition of neurotransmitter release via activation of presynaptic CB1Rs.

4.1. The validity of our data on presynaptic inhibition at PF-PC synapses induced by synthetic cannabinoids

In our experiments, WIN reduced PF-PC EPSC amplitude to 64.5% (1 μM) and 46.8% (10 μM) of the control value using P20–57 mice (Fig. 4D). These reductions are comparable to previously published values obtained from acute cerebellar slice preparations: 55.6% of control in 1 μM WIN (P15–21 rats) (Levenes et al., 1998), 29.1 and 12.3% in 1 and 5 μM WIN, respectively (P15–19 rats) (Takahashi and Linden, 2000), and 23.5% in 5 μM WIN (P9–14 mice) (Kawamura et al., 2006). The latter two reports show somewhat smaller percentages compared with our data, but this can be attributed to the differences in the ages of the animals used: an immunohistochemical study revealed that the distribution patterns of CB1Rs in the molecular layer show developmental changes (Kawamura et al., 2006).

Atwood et al. reported that the IC_{50} of JWH-018 against synaptic transmission is 14.9 nM using autaptic hippocampal neuronal cultures (Atwood et al., 2010), whereas our IC_{50} value for JWH-018 was approximately 100 times larger than that of their report (Table 1). This discrepancy might be explained by the different neuronal preparations used: Atwood et al. utilized dissociated neuronal cultures, whose synapses would not be wrapped by cell structures such as glial membranes. These synapses would be more easily exposed to CB1R agonists compared with those in cerebellar slice preparations, and therefore synaptic transmission in the autaptic hippocampal cultures might be suppressed by a lower concentration of JWH-018.

Using a binding assay for human recombinant CB1Rs, we recently found that relative IC_{50} s for WIN, MAM-2201, and JWH-018 against CB1Rs were 1.00, 0.70, and 5.30, respectively (Kikura-Hanjiri et al., manuscript in preparation). These data agree well with our observation of the relative IC_{50} s against excitatory neurotransmitter release from PF terminals to PCs using cerebellar slice preparations (Table 1). Therefore, we consider our observations of IC_{50} s in cerebellar preparations to be reasonable.

4.2. Adverse effects of MAM-2201 on targets of the cerebellar cortex and on cerebellum-dependent motor functions

PCs are the sole output GABAergic neurons from the cerebellar cortex and make direct synaptic contacts onto the deep cerebellar nuclear neurons and vestibular nuclear neurons (Voogd and Glickstein, 1998; Zheng and Raman, 2010). PCs receive two types of excitatory input from CFs and PFs. CFs arise from the inferior olivary complex located in the brainstem. CFs are activated during motor learning and induce complex spikes in PCs (Ito, 2001; Llinas et al., 2004). Spikelets in complex spike can propagate to the synaptic terminals of PCs (Khaliq and Raman, 2005). PFs are the axons of granule cells, which are excited by glutamatergic mossy fiber inputs. Mossy fibers originate from nuclei in the spinal cord and brain stem. The mossy fiber-PF pathway is the main operational input to the cerebellum and PCs, and carries afferent information both from the periphery and from other brain centers. PFs produce a brief excitatory postsynaptic potential in PCs that generates a single action potential called a “simple spike.” In addition, PCs receive feed-forward synaptic inhibition from GABAergic interneurons, and this inhibition increases the precision of PC spike outputs (Mittmann et al., 2005). Thus, all of these synaptic inputs to PCs can control the output of the cerebellar cortex. The absence of

PC activity or genetic manipulation of synaptic transmission from PCs severely affects cerebellum-dependent motor functions: both in mutant mice and in spinocerebellar ataxia type 6 patients, selective degeneration of PCs induce motor dysfunction (Frontali, 2001; Porras-Garcia et al., 2013), and PC-specific vesicular GABA transporter knockout mice exhibit motor impairment (Kayakabe et al., 2013).

We demonstrate that MAM-2201 inhibits neurotransmitter release at PF-PC, interneuron-PC, and CF-PC synapses in a concentration-dependent manner (Figs. 3–6), and reduces the number of spikelets in CF-evoked complex spikes (Fig. 7A and B). Assuming that, in humans, MAM-2201 inhibits neurotransmitter release at these synapses, the inhibition at PF-PC synapses could cause failure of simple spike generation in PCs. The inhibition of interneuron-PC synapses may weaken the feed-forward inhibition, leading to decreased precision of PC spike outputs. MAM-2201-induced reduction of spikelets in complex spikes (Fig. 7A and B) could cause a decrease in the number of action potentials that propagate to the synaptic terminals of PCs. Consequently, MAM-2201 may interrupt normal GABAergic inhibition onto the deep cerebellar nuclear neurons and vestibular nuclear neurons, and thus could affect cerebellum-dependent motor coordination. This speculation could be supported by the report that consumption of drugs of abuse containing analogs of MAM-2201 can cause cerebellar dysfunction such as disturbance of finger-to-finger test (Musshoff et al., 2014).

4.3. Possible effects of MAM-2201 on cerebellar LTD initiated by dendritic Ca^{2+} transients and on motor learning functions

PF-PC LTD is thought to underlie cerebellar motor learning in mammals (Yuzaki, 2012). This learning is impaired in transgenic mice that exhibit a deficit in the expression of LTD *in vitro* (Kakegawa et al., 2008). Induction of LTD requires association of PF and CF activation both *in vivo* and *in vitro* (Ito, 2001). At the cellular level, CF synaptic inputs to PCs evoke dendritic Ca^{2+} transients, which play crucial roles in the expression of LTD (Konnerth et al., 1992). Interestingly, Carey and Regehr reported that presynaptic inhibition of CF-PC synapses by noradrenaline alters the complex spike waveform and decreases CF-evoked dendritic Ca^{2+} transients, leading to interference with the induction of LTD (Carey and Regehr, 2009). This noradrenergic modulation shares many features with our observations of MAM-2201-induced changes of CF-evoked responses in PCs (Figs. 6 and 7): depression of CF-PC EPSCs via presynaptic mechanisms, reduction of the number of spikelets in complex spikes, and attenuation of CF-induced Ca^{2+} transients in PC dendrites. Taken together, MAM-2201 may interfere with the induction of LTD *in vitro* and might result in an impairment of cerebellar motor learning *in vivo*. Further work will be needed to clarify whether MAM-2201 indeed blocks the induction of LTD.

4.4. Implications for adverse effects of MAM-2201 on other brain functions

In the brain, CB1Rs are widely and abundantly expressed, and numerous *in vitro* studies have revealed that activation of CB1Rs by agonists suppresses synaptic transmission in several regions such as the hippocampus, nucleus accumbens, striatum, and cerebellar cortex (Kano et al., 2009). Moreover, in rat hippocampal slice preparations, pharmacological activation of CB1Rs modulates long-term potentiation in the CA1 region (Navakkode and Korte, 2014), and *in vivo* administration of WIN impairs hippocampal-dependent short-term memory (Hampson and Deadwyler, 2000). WIN also activates the “reward circuitry” in the brain, including the ventral tegmental area-nucleus accumbens pathway, and alters reward-

related behaviors in a similar manner to other reward-enhancing addictive drugs (Gardner, 2005). In this study, we demonstrated that MAM-2201 suppresses synaptic transmission in the cerebellum and that this action parallels that induced by WIN (Figs. 3–5). Taken together, in humans, MAM-2201 could cause psychoactive effects that are similar to those observed in the laboratory animal experiments using WIN or other synthetic cannabinoids.

Acknowledgments

This work was supported by Health Labour Sciences Research Grants. We thank Dr. Nobutake Hosoi (Gunma University) for technical advice on intracellular Ca^{2+} imaging.

References

- Atwood, B.K., Huffman, J., Straiker, A., Mackie, K., 2010. JWH018, a common constituent of 'Spice' herbal blends, is a potent and efficacious cannabinoid CB1 receptor agonist. *Br. J. Pharmacol.* 160, 585–593.
- Auwarter, V., Dresen, S., Weinmann, W., Muller, M., Putz, M., Ferreiros, N., 2009. 'Spice' and other herbal blends: harmless incense or cannabinoid designer drugs? *J. Mass Spectrom.* 44, 832–837.
- Brown, S.P., Safo, P.K., Regehr, W.G., 2004. Endocannabinoids inhibit transmission at granule cell to Purkinje cell synapses by modulating three types of presynaptic calcium channels. *J. Neurosci.* 24, 5623–5631.
- Bruno, A., Lembo, F., Novellino, E., Stornaiuolo, M., Marinelli, L., 2014. Beyond radiolabelled displacement techniques for identification of CB1 ligands: the first application of a fluorescence-quenching assay. *Sci. Rep.* 4, 3757.
- Carey, M.R., Regehr, W.G., 2009. Noradrenergic control of associative synaptic plasticity by selective modulation of instructive signals. *Neuron* 62, 112–122.
- Derungs, A., Schwaninger, A.E., Mansella, G., Bingisser, R., Kraemer, T., Liechti, M.E., 2013. Symptoms, toxicities, and analytical results for a patient after smoking herbs containing the novel synthetic cannabinoid MAM-2201. *Forensic Toxicol.* 31, 164–171.
- DeSanty, K.P., Dar, M.S., 2001. Cannabinoid-induced motor incoordination through the cerebellar CB(1) receptor in mice. *Pharmacol. Biochem. Behav.* 69, 251–259.
- Diana, M.A., Levenes, C., Mackie, K., Marty, A., 2002. Short-term retrograde inhibition of GABAergic synaptic currents in rat Purkinje cells is mediated by endogenous cannabinoids. *J. Neurosci.* 22, 200–208.
- Dousmanis, A.G., Pennefather, P.S., 1992. Inwardly rectifying potassium conductances in AtT-20 clonal pituitary cells. *Pflügers Arch.* 422, 98–104.
- Felder, C.C., Joyce, K.E., Briley, E.M., Glass, M., Mackie, K.P., Fahey, K.J., Cullinan, G.J., Hunden, D.C., Johnson, D.W., Chaney, M.O., Koppel, G.A., Brownstein, M., 1998. LY320135, a novel cannabinoid CB1 receptor antagonist, unmasks coupling of the CB1 receptor to stimulation of cAMP accumulation. *J. Pharmacol. Exp. Ther.* 284, 291–297.
- Frontali, M., 2001. Spinocerebellar ataxia type 6: channelopathy or glutamine repeat disorder? *Brain Res. Bull.* 56, 227–231.
- Gardner, E.L., 2005. Endocannabinoid signaling system and brain reward: emphasis on dopamine. *Pharmacol. Biochem. Behav.* 81, 263–284.
- Hagiwara, S., Miyazaki, S., Rosenthal, N.P., 1976. Potassium current and the effect of cesium on this current during anomalous rectification of the egg cell membrane of a starfish. *J. Gen. Physiol.* 67, 621–638.
- Hampson, R.E., Deadwyler, S.A., 2000. Cannabinoids reveal the necessity of hippocampal neural encoding for short-term memory in rats. *J. Neurosci.* 20, 8932–8942.
- Hashimoto, K., Kano, M., 2013. Synapse elimination in the developing cerebellum. *Cell. Mol. Life Sci.* 70, 4667–4680.
- Huestis, M.A., Gorelick, D.A., Heishman, S.J., Preston, K.L., Nelson, R.A., Moolchan, E.T., Frank, R.A., 2001. Blockade of effects of smoked marijuana by the CB1-selective cannabinoid receptor antagonist SR141716. *Arch. Gen. Psychiatry* 58, 322–328.
- Irie, T., Fukui, I., Ohmori, H., 2006. Activation of GIRK channels by muscarinic receptors and group II metabotropic glutamate receptors suppresses Golgi cell activity in the cochlear nucleus of mice. *J. Neurophysiol.* 96, 2633–2644.
- Irie, T., Matsuzaki, Y., Sekino, Y., Hirai, H., 2014. Kv3.3 channels harbouring a mutation of spinocerebellar ataxia type 13 alter excitability and induce cell death in cultured cerebellar Purkinje cells. *J. Physiol.* 592, 229–247.
- Irie, T., Ohmori, H., 2008. Presynaptic GABA(B) receptors modulate synaptic facilitation and depression at distinct synapses in fusiform cells of mouse dorsal cochlear nucleus. *Biochem. Biophys. Res. Commun.* 367, 503–508.
- Ito, M., 2001. Cerebellar long-term depression: characterization, signal transduction, and functional roles. *Physiol. Rev.* 81, 1143–1195.
- Kakegawa, W., Miyazaki, T., Emi, K., Matsuda, K., Kohda, K., Motohashi, J., Mishina, M., Kawahara, S., Watanabe, M., Yuzaki, M., 2008. Differential regulation of synaptic plasticity and cerebellar motor learning by the C-terminal PDZ-binding motif of GluRdelta2. *J. Neurosci.* 28, 1460–1468.
- Kano, M., Ohno-Shosaku, T., Hashimoto, Y., Uchigashima, M., Watanabe, M., 2009. Endocannabinoid-mediated control of synaptic transmission. *Physiol. Rev.* 89, 309–380.
- Kawamura, Y., Fukaya, M., Maejima, T., Yoshida, T., Miura, E., Watanabe, M., Ohno-Shosaku, T., Kano, M., 2006. The CB1 cannabinoid receptor is the major cannabinoid receptor at excitatory presynaptic sites in the hippocampus and cerebellum. *J. Neurosci.* 26, 2991–3001.
- Kayakabe, M., Kakizaki, T., Kaneko, R., Sasaki, A., Nakazato, Y., Shibasaki, K., Ishizaki, Y., Saito, H., Suzuki, N., Furuya, N., Yanagawa, Y., 2013. Motor dysfunction in cerebellar Purkinje cell-specific vesicular GABA transporter knockout mice. *Front. Cell. Neurosci.* 7, 286.
- Khalil, Z.M., Raman, I.M., 2005. Axonal propagation of simple and complex spikes in cerebellar Purkinje neurons. *J. Neurosci.* 25, 454–463.
- Kikura-Hanajiri, R., Uchiyama, N., Kawamura, M., Goda, Y., 2013. Changes in the prevalence of new psychoactive substances before and after the introduction of the generic scheduling of synthetic cannabinoids in Japan. *Drug Test. Anal.*
- Konnerth, A., Dreessen, J., Augustine, G.J., 1992. Brief dendritic calcium signals initiate long-lasting synaptic depression in cerebellar Purkinje cells. *Proc. Natl. Acad. Sci. U. S. A.* 89, 7051–7055.
- Korn, H., Faber, D.S., 1991. Quantal analysis and synaptic efficacy in the CNS. *Trends Neurosci.* 14, 439–445.
- Kreitzer, A.C., Regehr, W.G., 2001. Retrograde inhibition of presynaptic calcium influx by endogenous cannabinoids at excitatory synapses onto Purkinje cells. *Neuron* 29, 717–727.
- Kubo, Y., Reuveny, E., Slesinger, P.A., Jan, Y.N., Jan, L.Y., 1993. Primary structure and functional expression of a rat G-protein-coupled muscarinic potassium channel. *Nature* 364, 802–806.
- Kushmerick, C., Price, G.D., Taschenberger, H., Puente, N., Renden, R., Wadiche, J.L., Duvoisin, R.M., Grandes, P., von Gersdorff, H., 2004. Retroinhibition of presynaptic Ca^{2+} currents by endocannabinoids released via postsynaptic mGluR activation at a calyx synapse. *J. Neurosci.* 24, 5955–5965.
- Levenes, C., Daniel, H., Soubrie, P., Crepel, F., 1998. Cannabinoids decrease excitatory synaptic transmission and impair long-term depression in rat cerebellar Purkinje cells. *J. Physiol.* 510 (Pt 3), 867–879.
- Linas, R., Walton, K.D., Lang, E.J., 2004. Cerebellum. In: Shepard, G.M. (Ed.), *The Synaptic Organization of the Brain*, fifth ed. Oxford University Press, New York, NY, US, pp. 271–309.
- Lonati, D., Buscaglia, E., Papa, P., Valli, A., Coccini, T., Giampreti, A., Petrolini, V.M., Vecchio, S., Serpelloni, G., Locatelli, C.A., 2014. MAM-2201 (analytically confirmed) intoxication after "synthacaine" consumption. *Ann. Emerg. Med.*
- Luk, T., Jin, W., Zvonok, A., Lu, D., Lin, X.Z., Chavkin, C., Makriyannis, A., Mackie, K., 2004. Identification of a potent and highly efficacious, yet slowly desensitizing CB1 cannabinoid receptor agonist. *Br. J. Pharmacol.* 142, 495–500.
- Mackie, K., 2008. Signaling via CNS cannabinoid receptors. *Mol. Cell. Endocrinol.* 286, S60–S65.
- Mackie, K., Lai, Y., Westenbroek, R., Mitchell, R., 1995. Cannabinoids activate an inwardly rectifying potassium conductance and inhibit Q-type calcium currents in AtT20 cells transfected with rat brain cannabinoid receptor. *J. Neurosci.* 15, 6552–6561.
- Maejima, T., Hashimoto, K., Yoshida, T., Aiba, A., Kano, M., 2001. Presynaptic inhibition caused by retrograde signal from metabotropic glutamate to cannabinoid receptors. *Neuron* 31, 463–475.
- McKay, B.E., Turner, R.W., 2005. Physiological and morphological development of the rat cerebellar Purkinje cell. *J. Physiol.* 567, 829–850.
- Mittmann, W., Koch, U., Hausser, M., 2005. Feed-forward inhibition shapes the spike output of cerebellar Purkinje cells. *J. Physiol.* 563, 369–378.
- Monory, K., Blanduzun, H., Massa, F., Kaiser, N., Lemberger, T., Schutz, G., Wotjak, C.T., Lutz, B., Marsicano, G., 2007. Genetic dissection of behavioural and autonomic effects of Delta(9)-tetrahydrocannabinol in mice. *PLoS Biol.* 5, e269.
- Moosmann, B., Kneisel, S., Girreser, U., Brecht, V., Westphal, F., Auwarter, V., 2012. Separation and structural characterization of the synthetic cannabinoids JWH-412 and 1-[(5-fluoropentyl)-1H-indol-3-yl]-4-methylnaphthalen-1-ylmethanone using GC-MS, NMR analysis and a flash chromatography system. *Forensic Sci. Int.* 220, e17–22.
- Musshoff, F., Madea, B., Kernbach-Wighton, G., Bicker, W., Kneisel, S., Hutter, M., Auwarter, V., 2014. Driving under the influence of synthetic cannabinoids ("Spice"): a case series. *Int. J. Legal Med.* 128, 59–64.
- Navakkode, S., Korte, M., 2014. Pharmacological activation of CB1 receptor modulates long term potentiation by interfering with protein synthesis. *Neuropharmacology* 79, 525–533.
- Patel, S., Hillard, C.J., 2001. Cannabinoid CB(1) receptor agonists produce cerebellar dysfunction in mice. *J. Pharmacol. Exp. Ther.* 297, 629–637.
- Porrás-García, M.E., Ruiz, R., Pérez-Villegas, E.M., Armengol, J.A., 2013. Motor learning of mice lacking cerebellar Purkinje cells. *Front. Neuroanat.* 7, 4.
- Regehr, W.G., Carey, M.R., Best, A.R., 2009. Activity-dependent regulation of synapses by retrograde messengers. *Neuron* 63, 154–170.
- Safo, P.K., Cravatt, B.F., Regehr, W.G., 2006. Retrograde endocannabinoid signaling in the cerebellar cortex. *Cerebellum* 5, 134–145.
- Safo, P.K., Regehr, W.G., 2005. Endocannabinoids control the induction of cerebellar LTD. *Neuron* 48, 647–659.
- Saito, T., Namera, A., Miura, N., Ohta, S., Miyazaki, S., Osawa, M., Inokuchi, S., 2013. A fatal case of MAM-2201 poisoning. *Forensic Toxicol.* 31, 333–337.
- Seely, K.A., Lapoint, J., Moran, J.H., Fattore, L., 2012. Spice drugs are more than harmless herbal blends: a review of the pharmacology and toxicology of synthetic cannabinoids. *Prog. Neuro Psychopharmacol. Biol. Psychiatry* 39, 234–243.

- Shen, M., Thayer, S.A., 1999. Delta9-tetrahydrocannabinol acts as a partial agonist to modulate glutamatergic synaptic transmission between rat hippocampal neurons in culture. *Mol. Pharmacol.* 55, 8–13.
- Showalter, V.M., Compton, D.R., Martin, B.R., Abood, M.E., 1996. Evaluation of binding in a transfected cell line expressing a peripheral cannabinoid receptor (CB2): identification of cannabinoid receptor subtype selective ligands. *J. Pharmacol. Exp. Ther.* 278, 989–999.
- Shuvaev, A.N., Horiuchi, H., Seki, T., Goenawan, H., Irie, T., Iizuka, A., Sakai, N., Hirai, H., 2011. Mutant PKC(γ) in spinocerebellar ataxia type 14 disrupts synapse elimination and long-term depression in Purkinje cells in vivo. *J. Neurosci.* 31, 14324–14334.
- Szabo, B., Than, M., Thorn, D., Wallmichrath, I., 2004. Analysis of the effects of cannabinoids on synaptic transmission between basket and Purkinje cells in the cerebellar cortex of the rat. *J. Pharmacol. Exp. Ther.* 310, 915–925.
- Takahashi, K.A., Linden, D.J., 2000. Cannabinoid receptor modulation of synapses received by cerebellar Purkinje cells. *J. Neurophysiol.* 83, 1167–1180.
- Taura, F., Sirikantaramas, S., Shoyama, Y., Shoyama, Y., Morimoto, S., 2007. Phytocannabinoids in *Cannabis sativa*: recent studies on biosynthetic enzymes. *Chem. Biodivers.* 4, 1649–1663.
- Uchiyama, N., Kawamura, M., Kikura-Hanajiri, R., Goda, Y., 2013. URB-754: a new class of designer drug and 12 synthetic cannabinoids detected in illegal products. *Forensic Sci. Int.* 227, 21–32.
- Vardakou, I., Pistos, C., Spiliopoulou, C., 2010. Spice drugs as a new trend: mode of action, identification and legislation. *Toxicol. Lett.* 197, 157–162.
- Vincent, P., Marty, A., 1996. Fluctuations of inhibitory postsynaptic currents in Purkinje cells from rat cerebellar slices. *J. Physiol.* 494 (Pt 1), 183–199.
- Voogd, J., Glickstein, M., 1998. The anatomy of the cerebellum. *Trends Cogn. Sci.* 2, 307–313.
- Wilson, R.I., Nicoll, R.A., 2002. Endocannabinoid signaling in the brain. *Science* 296, 678–682.
- Xu-Friedman, M.A., Regehr, W.G., 1999. Presynaptic strontium dynamics and synaptic transmission. *Biophys. J.* 76, 2029–2042.
- Yuzaki, M., 2012. Cerebellar LTD vs. motor learning—lessons learned from studying GluD2. *Neural Netw.*
- Zheng, N., Raman, I.M., 2010. Synaptic inhibition, excitation, and plasticity in neurons of the cerebellar nuclei. *Cerebellum* 9, 56–66.
- Zucker, R.S., Regehr, W.G., 2002. Short-term synaptic plasticity. *Annu Rev. Physiol.* 64, 355–405.

ミクログリアの発生と分化

佐藤 薫

ミクログリアの発生と分化過程

脳の免疫機能担当細胞として長らく知られてきたミクログリアは脳細胞の5%を占める。Macrophage 1 antigen (Mac1), major histocompatibility complex (MHC) class II, CD68, F4/80 や fragment, crystallizable (Fc) 受容体, low density lipoprotein (LDL) 受容体といった細胞表面抗原を発現していること、貪食能, サイトカイン分泌といった機能を有することなど, モノサイトやマクロファージに類似点が多いため, 脳内炎症レベルの決定細胞として長らく炎症を伴う病態研究の対象となってきた。ミクログリアをモノサイトやマクロファージと決定的に区別できる細胞表面抗原がまだ見つかっていないため, その起源についてもモノサイトやマクロファージと共通であると長らく考えられてきた。しかし2010~12年にかけて, ミクログリアが系統的に発生過程の早い時期にマクロファージと分かれていることが明らかにされた。ミクログリアは胎生7.5日齢に骨髄前駆細胞から分化し胎生8.5~9.5日齢にはすでに脳内に移行している^{1,2)}。Ginhouxらは, 造血幹細胞(モノサイトやマクロファージのもとになる幹細胞)の完成前である胎生7日齢に, ミクログリア前駆細胞がすでに卵黄嚢で発生しており, 胎生9日齢までにこれらの細胞が脳に移行してミクログリアとなることを実験的に証明した¹⁾。これは神経幹細胞であるラジアルグリアが脳内に発生する(胎生10.5日齢)よりも早いタイミングの出来事である。このミクログリア前駆細胞はCsf1受容体を発現したMyb(-), PU.1依存性であることも²⁾, Myb(+)な造血幹細胞とは異なる点である。一方, 病態時には血液脳関門のバリア機能低下により血球系細胞の脳内浸潤が起こるが, これらの細胞がミクログリアにはならないことも示されている。モノサイトやマクロファージのみがgreen fluorescent protein (GFP) 標識されたマウスに実験的脳脊髄炎(experimental allergic encephalomyelitis: EAE)を発症さ

せると, EAE症状の重篤度に応じてモノサイトが脊髄に浸潤するが, 炎症終息後にGFP陽性細胞は消失した³⁾。以上のことから, 脳内で生理的な機能を持つミクログリアのほとんどが胎生7.5日齢に脳内に移行したミクログリア前駆細胞の子孫たちであると考えられる。ところが, このように共通の先祖を持ちながらミクログリアは中枢神経系の発達, 機能分化とともに, ミエリン, 血管系, 血液脳関門, 周囲細胞の細胞外マトリックス, 神経伝達物質, といった周囲環境との相互作用によって, その領域, その時期に特異的な形態, 抗原発現パターン, 増殖パターン, 生理機能を獲得する^{4,5)}。さらに言えば, 一領域中のミクログリア集団の中に感染や外傷に対して非常に劇的に反応する集団とそうでない集団が含まれていることもあり⁶⁾, ミクログリアと微細な周囲環境との相互作用が起こっていると考えられる。

ミクログリアは, 正常脳でよくみられるような, 細かく発達した多くの突起を持つ「静止型」と神経炎症等の病変部に集積しているアメボイド状の「活性化型」との間を環境の変化に応じて行き来する細胞である。しかし最近の研究で, 静止型ミクログリアはその発達した突起により周囲環境を実に積極的に探索していることが明らかとなっている⁵⁾。したがって「静止型」, 「活性化型」はもはや言葉通りに捉えきれなくなっている。現在, ミクログリアの活性状態はM0, M1, M2ステージというカテゴリーで表現されるが, この概念はそもそもマクロファージ研究から導入された⁷⁾。マクロファージは外部刺激に対する反応によってM1, M2a, M2b, M2cというカテゴリーに分けられるが⁸⁾, ミクログリアと異なる点は, 分類に有効な35種類の表面抗原が明らかになっている点である。M1ミクログリアは炎症誘発特性, M2ミクログリアが抗炎症特性を持つ, と言われるが, そのどちらにも入らないM0ミクログリアという集団も発見されている⁴⁾。M1, M2の間とも言えるミクログリアも存在する。生後初期マウスのミクログリアはM1遺伝子(iNOS, TNF α)とM2遺伝子(Arginase-1)の両者を高発現している。M0, M1, M2ステージの他に

さとう かおる 国立医薬品食品衛生研究所薬理部第一室長(中枢神経薬理)

HoxB8 というホメオボックスタンパク質の発現によってミクログリアを分類しているグループもいる⁹⁾。HoxB8 (+)細胞は CD11b (+)ミクログリアの 15%を占め、卵黄嚢から分化するミクログリアとは異なる細胞集団であると報告されている。HoxB8 を欠損したマウスは強迫性障害スペクトラムに伴う脱毛症と非常によく似た症状が現れるため、病態解明への応用が期待されている。

脳室下帯ミクログリアに関する最近の知見

脳室帯 (ventricular zone : VZ) と脳室下帯 (subventricular zone : SVZ) は一生を通じて神経新生やグリア新生が起こる領域であることが明らかとなつて久しい。主要な投射神経は胎生期に、アストロサイトは胎生期から生後初期まで、オリゴデンドロサイトは胎生後期から生後初期にかけて、介在神経は胎生後期以降新生される¹⁰⁾。一方、上で述べたように胎生 8.5~9.5 日齢にはアメボイド型のミクログリアが脳内にすでに存在している^{1,2)}。ミクログリアは生後初期に爆発的に増加するが¹¹⁾、発達が進むにつれアメボイド型のミクログリアは減少し成体においてほとんど静止型になる¹²⁾。しかし、胎生期の神経新生にミクログリアがどのように関わっているかについては 2013 年に Cunningham らが報告するまで、ほとんどわかっていなかった¹³⁾。彼らは胎生期の脳皮質神経細胞新生過程の後半において、ミクログリアが貪食作用によって神経前駆細胞プールの細胞数を調節していることを明らかにした。このとき、ミクログリアが貪食した細胞はアポトーシスを起こしていない点は興味深い。成体海馬歯状回顆粒細胞層 (subgranular zone : SGZ) での神経新生の場合、ミクログリアはアポトーシスを起こした細胞を貪食しているからである¹⁴⁾。発達期 SVZ と成体 SGZ での神経新生とミクログリアの関連について、さらなる解明が待たれる。

生後 SVZ の神経新生におけるミクログリアの役割については胎生期に増してほとんど情報がなかったが、2006 年に、SVZ のように神経新生が活発な領域とそれ以外の領域とでミクログリアの活性化や機能に差があることが指摘された¹⁵⁾。最近われわれは、生後初期に活性化型ミクログリアが SVZ に一過的に集積しており、成熟に伴い、より突起の発達したミクログリアが白質まで分散するようになることを見出した。われわれは生後初期 SVZ でこのように特

異な挙動を示すミクログリアが、SVZ における神経新生およびオリゴデンドロサイト新生を促進することを明らかにした¹⁶⁾ (図 1)。SVZ は一生を通じて神経新生が継続するものの、年を重ねるにつれ新生細胞数は激減する。われわれのデータでも、生後 30 日齢の SVZ に活性化型ミクログリアはすでにほとんど存在せず、SVZ 神経新生動態と相関がある。興味深いことに、SVZ での神経新生に対するミクログリアの作用は SVZ 中の位置によって異なるようである。われわれも体軸の中間あたり、線条体と海馬が対面するあたりが最もミクログリア密度が高いことを見出している。この細胞分布の偏りは血管系が関与している可能性がある。血管は成体脳 SVZ において神経新生ニッチとなることが知られているが^{17,18)}、SVZ は血管叢と呼ばれるほど血管が発達しており^{19,20)}、特に SVZ 中心部は腹側から大きな血管が来ている^{20,21)}。血管から多種の液性因子が放出されていることはよく知られているが¹⁷⁾、大脳皮質にミクログリアが移行するのに重要なシグナルカスケードである CXCL12/CXCR4 シグナル²²⁾の関与などが考えられる。成体脳における脳室上衣下層 (subependymal zone : SEZ) では吻側尾側方向、背側腹側方向に高度に領域化されており、各領域からは異なる神経細胞系列が新生してくることも知られている²³⁾。また、背側 SEZ ではより多くのオリゴデンドロサイト新生が起こることも知られている²⁴⁾。今後、SVZ 領域をさらに細分化してミクログリアの役割について検討する必要があるだろう。

成体脳 SVZ からとってきた神経幹細胞や神経前駆細胞の場合、Th2 ヘルパー T 細胞由来サイトカインによって刺激されたミクログリアが神経新生やオリゴデンドロサイト新生を促進する²⁵⁾。このとき、ミクログリアから放出される IGF-1 が作用に関与していることが示唆されている。しかし、生後初期 SVZ においては IGF-1 を発現しているミクログリアはわずかに確認されるが、IGF-1 はミクログリアの神経新生促進作用の作用本体ではなかった¹⁶⁾。われわれは、ミクログリアが神経新生、オリゴデンドロサイト新生を促進するメカニズムとして生後 4~9 日齢の SVZ において一過的に濃度が上昇するサイトカイン群 (IL-1 β , IL-6, TNF α , IFN γ) が重要であることを明らかとした。興味深いのは、神経幹細胞塊 (neurosphere) とミクログリアの共培養系を用いた実験で、上記 4 種のサイトカインのう

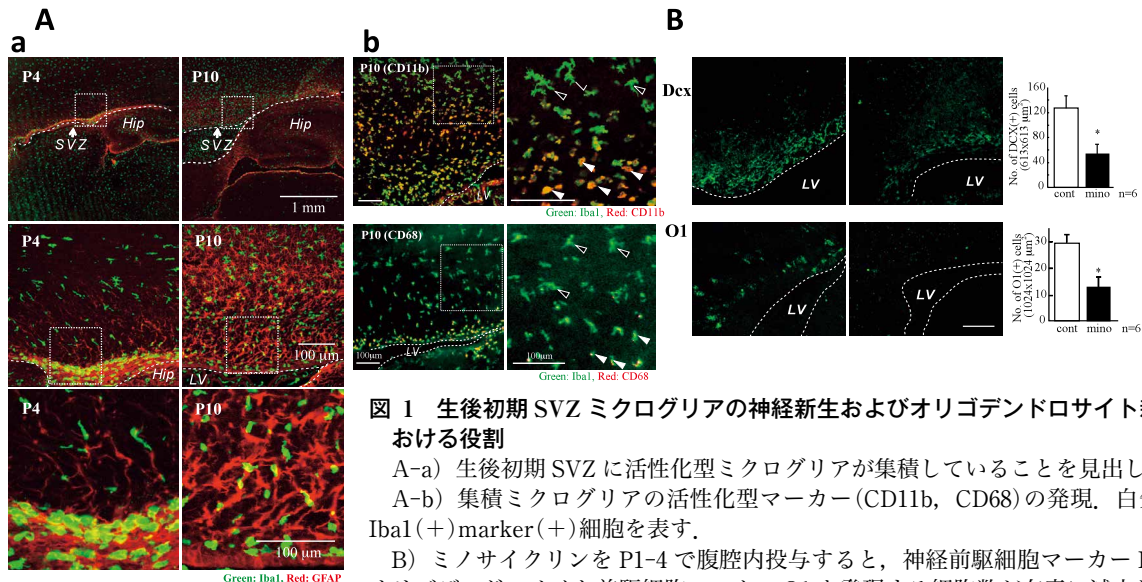


図 1 生後初期 SVZ ミクログリアの神経新生およびオリゴデンドロサイト新生における役割

A-a) 生後初期 SVZ に活性化型ミクログリアが集積していることを見出した。
 A-b) 集積ミクログリアの活性化型マーカー (CD11b, CD68) の発現。白矢頭は Iba1 (+) marker (+) 細胞を表す。
 B) ミノサイクリンを P1-4 で腹腔内投与すると、神経前駆細胞マーカー Dcx とオリゴデンドロサイト前駆細胞マーカー O1 を発現する細胞数が有意に減少した。
 * $p < 0.05$ vs. control group, student's t test ($N=6$). (Shigemoto-Mogami ら¹⁶) より改変)

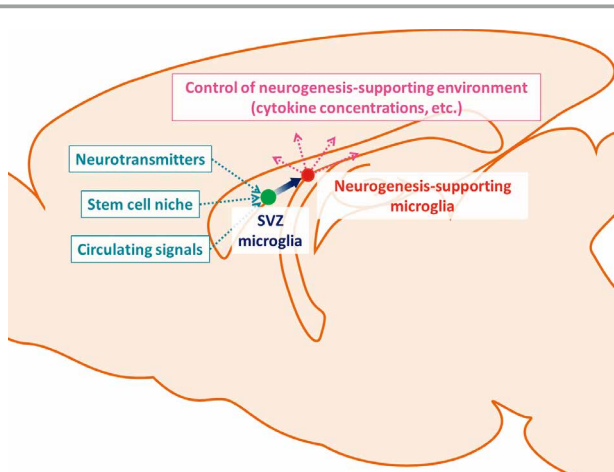


図 2

SVZ ミクログリアは脳内・脳外環境からの信号に応じてサイトカイン環境を調節する 'Hub' として機能しているのではないかと示唆している。

ち 1 種のサイトカイン機能を機能中和抗体で阻害してもミクログリアの作用に何ら影響はなかったが、全てのサイトカインを同時に阻害するとミクログリアの作用が消失したことである。この結果は神経新生やオリゴデンドロサイト新生を複数のサイトカインが相補的に促進していることを示唆している。これまで、神経新生に関するサイトカイン

の作用としては、神経前駆細胞が IL-1 β , IL-1R1, IL-1R2 を発現し、IL-1 β は神経前駆細胞の増殖と分化を調節していること²⁶、IL-6 が IL-6R を介して神経新生を促進すること²⁷などが報告されていたが、複数サイトカインによる相補的な作用は報告がなかった。Li らは IFN γ の作用はミクログリア存在下では表現系が異なることを示しており、われわれが示した相補的作用を支持するものである²⁸。そもそも、IL-1 β , IL-6, TNF α , IFN γ は炎症性サイトカインとして、LPS (lipopolysaccharide) 刺激²⁹、EAE³⁰、status epilepticus (SE)³¹ といった病理的条件下では神経新生を抑制する本体として研究されてきた。しかし、より穏やかな実験条件下では異なる作用が発揮される。炎症モデル作成のために使われる LPS は、適用条件 (適用時間など) をわずかに調整することでミクログリアの神経新生への影響が変化する³²。サイトカイン自身も濃度によって作用が変化する。TNF α は 1 ng/mL では神経幹細胞を増殖する一方、10 ng/mL 以上の濃度でアポトーシスを起こす³³。われわれのデータでは、ミノサイクリンがミクログリアの活性化を抑制すると、神経前駆細胞の数は半分以下に減少するのに対し、それぞれのサイトカインレベルの減少は皆一様に穏やかであった。サイトカインはミクログリアだけでなく

アストロサイトなどの周囲細胞からも放出される。おそらく、ミクログリアからのサイトカイン放出が‘cytokine storm’³⁴⁾には遠く及ばない程度の、‘cytokine drizzling’とも言える連続的なサイトカイン放出トリガーとなっていることが予想される。

むすび

われわれにとって次の課題は、生後初期ミクログリアの活性化機構の解明である。重大なヒントとして胎生期から生後にかけてSVZでのミクログリア機能が大きく変化する点があげられる。体内を循環している種々のメディエーターは誕生の前後で質、量ともに大きく変化する³⁵⁾。われわれは、SVZミクログリアはこのような脳内・脳外環境からの信号に応じてサイトカイン環境を調節する‘Hub’として機能しているのではないかと考えている(図2)。このような脳外から脳内への情報デリバリー、それに伴うミクログリアによる神経新生の調節メカニズムの解明は、発達障害を含む神経障害治療にもブレークスルーをもたらすことが期待される。

文 献

- 1) Ginhoux F, Greter M, Leboeuf M, et al. Fate mapping analysis reveals that adult microglia derive from primitive macrophages. *Science*. 2010 ; 330 : 841-5.
- 2) Schulz C, Gomez Perdiguero E, Chorro L, et al. A lineage of myeloid cells independent of Myb and hematopoietic stem cells. *Science*. 2012 ; 336 : 86-90.
- 3) Ajami B, Bennett JL, Krieger C, et al. Infiltrating monocytes trigger EAE progression, but do not contribute to the resident microglia pool. *Nat Neurosci*. 2011 ; 14 : 1142-9.
- 4) Butovsky O, Jedrychowski MP, Moore CS, et al. Identification of a unique TGF- β -dependent molecular and functional signature in microglia. *Nat Neurosci*. 2014 ; 17 : 131-43.
- 5) Kettenmann H, Hanisch UK, Noda M, Verkhratsky A. Physiology of microglia. *Physiol Rev*. 2011 ; 91 : 461-553.
- 6) Scheffel J, Regen T, Van Rossum D, et al. Toll-like receptor activation reveals developmental reorganization and unmasks responder subsets of microglia. *Glia*. 2012 ; 60 : 1930-43.
- 7) Sica A, Mantovani A. Macrophage plasticity and polarization : in vivo veritas. *J Clin Invest*. 2012 ; 122 : 787-95.
- 8) Geissmann F, Gordon S, Hume DA, et al. Unravelling mononuclear phagocyte heterogeneity. *Nat Rev Immunol*. 2010 ; 10 : 453-60.
- 9) Chen SK, Tvrdik P, Peden E, et al. Hematopoietic origin of pathological grooming in Hoxb8 mutant mice. *Cell*. 2010 ; 141 : 775-85.
- 10) Wang DD, Bordey A. The astrocyte odyssey. *Prog Neurobiol*. 2008 ; 86 : 342-67.
- 11) Sminia T, de Groot CJ, Dijkstra CD, et al. Macrophages in the central nervous system of the rat. *Immunobiology*. 1987 ; 174 : 43-50.
- 12) Zusso M, Methot L, Lo R, et al. Regulation of postnatal forebrain amoeboid microglial cell proliferation and development by the transcription factor Runx1. *J Neurosci*. 2012 ; 32 : 11285-98.

- 13) Cunningham CL, Martínez-Cerdeño V, Noctor SC. Microglia regulate the number of neural precursor cells in the developing cerebral cortex. *J Neurosci*. 2013 ; 33 : 4216-33.
- 14) Sierra A, Encinas JM, Deudero JJ, et al. Microglia shape adult hippocampal neurogenesis through apoptosis-coupled phagocytosis. *Cell Stem Cell*. 2010 ; 7 : 483-95.
- 15) Goings GE, Kozłowski DA, Szele FG. Differential activation of microglia in neurogenic versus non-neurogenic regions of the forebrain. *Glia*. 2006 ; 54 : 329-42.
- 16) Shigemoto-Mogami Y, Hoshikawa K, Goldman JE, et al. Microglia enhance neurogenesis and oligodendrogenesis in the early postnatal subventricular zone. *J Neurosci*. 2014 ; 34 : 2231-43.
- 17) Goldberg JS, Hirschi KK. Diverse roles of the vasculature within the neural stem cell niche. *Regen Med*. 2009 ; 4 : 879-97.
- 18) Quaegebeur A, Lange C, Carmeliet P. The neurovascular link in health and disease : molecular mechanisms and therapeutic implications. *Neuron*. 2011 ; 71 : 406-24.
- 19) Ihrie RA, Alvarez-Buylla A. Lake-front property : a unique germinal niche by the lateral ventricles of the adult brain. *Neuron*. 2011 ; 70 : 674-86.
- 20) Shen Q, Wang Y, Kokovay E, et al. Adult SVZ stem cells lie in a vascular niche : a quantitative analysis of niche cell-cell interactions. *Cell Stem Cell*. 2008 ; 3 : 289-300.
- 21) Dorr A, Sled JG, Kabani N. Three-dimensional cerebral vasculature of the CBA mouse brain : a magnetic resonance imaging and micro computed tomography study. *Neuroimage*. 2007 ; 35 : 1409-23.
- 22) Arnò B, Grassivaro F, Rossi C, et al. Neural progenitor cells orchestrate microglia migration and positioning into the developing cortex. *Nat Commun*. 2014 ; 5 : 5611.
- 23) Merkle FT, Mirzadeh Z, Alvarez-Buylla A. Mosaic organization of neural stem cells in the adult brain. *Science*. 2007 ; 317 : 381-4.
- 24) Ortega F, Gascon S, Masserdotti G, et al. Oligodendroglial and neurogenic adult subependymal zone neural stem cells constitute distinct lineages and exhibit differential responsiveness to Wnt signalling. *Nat Cell Biol*. 2013 ; 15 : 602-13.
- 25) Butovsky O, Ziv Y, Schwartz A, et al. Microglia activated by IL-4 or IFN- γ differentially induce neurogenesis and oligodendrogenesis from adult stem/progenitor cells. *Mol Cell Neurosci*. 2006 ; 31 : 149-60.
- 26) Wang X, Fu S, Wang Y, et al. Interleukin-1 β mediates proliferation and differentiation of multipotent neural precursor cells through the activation of SAPK/JNK pathway. *Mol Cell Neurosci*. 2007 ; 36 : 343-54.
- 27) Islam O, Gong X, Rose-John S, Heese K. Interleukin-6 and neural stem cells : more than gliogenesis. *Mol Biol Cell*. 2009 ; 20 : 188-99.
- 28) Li L, Walker TL, Zhang Y, et al. Endogenous interferon gamma directly regulates neural precursors in the non-inflammatory brain. *J Neurosci*. 2010 ; 30 : 9038-50.
- 29) Monje ML, Toda H, Palmer TD. Inflammatory blockade restores adult hippocampal neurogenesis. *Science*. 2003 ; 302 : 1760-5.
- 30) Ben-Hur T, Ben-Menachem O, Furer V, et al. Effects of proinflammatory cytokines on the growth, fate, and motility of multipotent neural precursor cells. *Mol Cell Neurosci*. 2003 ; 24 : 623-31.
- 31) Iosif RE, Ekdahl CT, Ahlenius H, et al. Tumor necrosis factor receptor 1 is a negative regulator of progenitor proliferation in adult hippocampal neurogenesis. *J Neurosci*. 2006 ; 26 : 9703-12.
- 32) Cacci E, Ajmone-Cat MA, Anelli T, et al. In vitro neuronal and glial differentiation from embryonic or adult neural precursor cells are differently affected by chronic or acute activation of microglia. *Glia*. 2008 ; 56 : 412-25.
- 33) Bernardino L, Agasse F, Silva B, et al. Tumor necrosis factor- α modulates survival, proliferation, and neuronal differentiation in neonatal subventricular zone cell cultures. *Stem Cells*. 2008 ; 26 : 2361-71.
- 34) Clark IA. The advent of the cytokine storm. *Immunol Cell Biol*. 2007 ; 85 : 271-3.
- 35) Spencer SJ, Mouihate A, Galic MA, Pittman QJ. Central and peripheral neuroimmune responses : hyporesponsiveness during pregnancy. *J Physiol*. 2008 ; 586 : 399-406.

Improvements in Enzyme-Linked Photoassay Systems for Spatiotemporal Observation of Neurotransmitter Release

Kazunori Watanabe, Nobuto Takahashi, Naohiro Hozumi¹ and Sachiko Yoshida*

Department of Environmental and Life Sciences,
Toyohashi University of Technology, 1-1 Hibarigaoka, Tempaku-cho, Toyohashi 441-8580, Japan
¹Int'l Cooperation Center for Engineering Education Development/
Department of Electrical & Electronic Information Engineering,
Toyohashi University of Technology, 1-1 Hibarigaoka, Tempaku-cho, Toyohashi 441-8580, Japan

(Received February 23, 2015; accepted September 25, 2015)

Key words: neurotransmitter, glutamate, GABA, enzyme immobilization, UV LED

Neurotransmitters and neuronal releasing molecules are not only the regulators of neuronal function but also the indicators of neuronal conditions. Glutamate and γ -amino butyric acid (GABA) play important roles in cerebellar differentiation and function. In the mature cortex, they are released from synapses and taken up by transporter molecules. We have developed enzyme-linked photoassay systems for glutamate, GABA, and adenosine triphosphate (ATP), and reported their release in the developing cerebellar cortex. Our systems showed slow transmitter release in the immature cerebellum, whereas it was hard to detect the fast synaptic release from mature neurons, because there were some limitations in time resolution and data depth derived from a charge-coupled device (CCD), and the enzyme-linked photodevice was sometimes unstable. In this study, we report the dynamic observation of neurotransmitter release in the developing cerebellar slices using improved photodevices and a high-speed 16-bit CCD. With this new system, the rapid measurement of transmitter release in a young-adult cerebellar cortex is possible. We suggest that these photoassay systems are useful for observing synaptic release in several diseases.

1. Introduction

Neurotransmitter molecules released from neurons are not only the regulators of neuronal transduction but also the indicators of neuronal conditions.⁽¹⁻³⁾ Glutamate and γ -aminobutyric acid (GABA) are known as typical transmitters in the brain's cortex, and they play important roles as stimulators and suppressors, respectively. Lack of balance in the release of glutamate and GABA may lead to autism, epilepsy, or Parkinson's disease.⁽⁴⁾

*Corresponding author: e-mail: syoshida@ens.tut.ac.jp

To observe spatiotemporal neurotransmitter release in the cerebellar cortex, we have recently developed an enzyme-linked photoassay system, which is a device with an immobilized enzyme on a quartz glass surface. Using this system, we observed glutamate or GABA release in developing cerebellar slices using either new or authorized methods.⁽⁵⁾ Enzyme-linked photoassay is sensitive and selective, and it can discriminate the substrates from their pharmacological analogues. Our system can detect transmitter release in the cerebral cortex,⁽⁶⁾ hippocampus, retina, and cultured cells,⁽⁷⁾ and made it possible to detect the release of adenosine triphosphate (ATP),⁽⁸⁾ glucose, sucrose, and fructose. On the other hand, enzymes tend to denature and separate from the quartz. For the detection of transmitter release in mature neuronal circuits, increasing the sensitivity and stability of the device is required.

In this paper, we propose new immobilizing methods and discuss the optimization of the enzyme-linked photoassay.

2. Materials and Methods

2.1 Substrate and enzyme reaction

Imaging neurotransmitter release was monitored for the reaction in which oxidoreductases generate reduced nicotinamide adenine dinucleotide (NAD^+) or diphosphonucleotide (NADP^+). For glutamate, GABA, or adenosine triphosphate (ATP) imaging, we used glutamate dehydrogenase, GABA disassembly enzyme [GABase, Fig. 1(a)] or glyceraldehyde 3-phosphate dehydrogenase, respectively.^(9–11) The NADH or NADPH, the reductants of NAD^+ or NADP^+ , respectively, which is generated stoichiometrically, emits 480 nm fluorescence after excitation at 340–365 nm.

2.2 Surface photoexcitation

For UV excitation, a quartz glass plate illuminated with an ultraviolet light-emitting diode (UV-LED, Nichia, Tokushima, Japan) was used. Leaking UV light onto the glass surface excited fluorescent NADH or NADPH [Fig. 1(b)].

2.3 Imaging apparatus

All fluorescence images through the inverted microscope (IX73, Olympus Co., Ltd., Tokyo, Japan) were observed by a cooled charge-coupled device (CCD) (ORCA-ER CCD) or a high-speed complimentary metal-oxide semiconductor (CMOS) (ORCA-Flash 4.0) camera, supplied by Hamamatsu Photonics Co., Ltd., Hamamatsu, Japan. Imaging data were analyzed by iVision software (BD Biosciences, San Jose, CA, USA).

2.4 Enzyme immobilization and sample preparation

Enzymes were typically covalently immobilized on the quartz glass surface using a silane coupling agent and a crosslinking agent, 3-aminopropyltriethoxy silane (3-APTS) and glutaraldehyde, respectively [Fig. 2(a)].⁽¹²⁾ These surface modifications determine both the stability of the enzyme reaction and the distance between the sample and the glass surface.

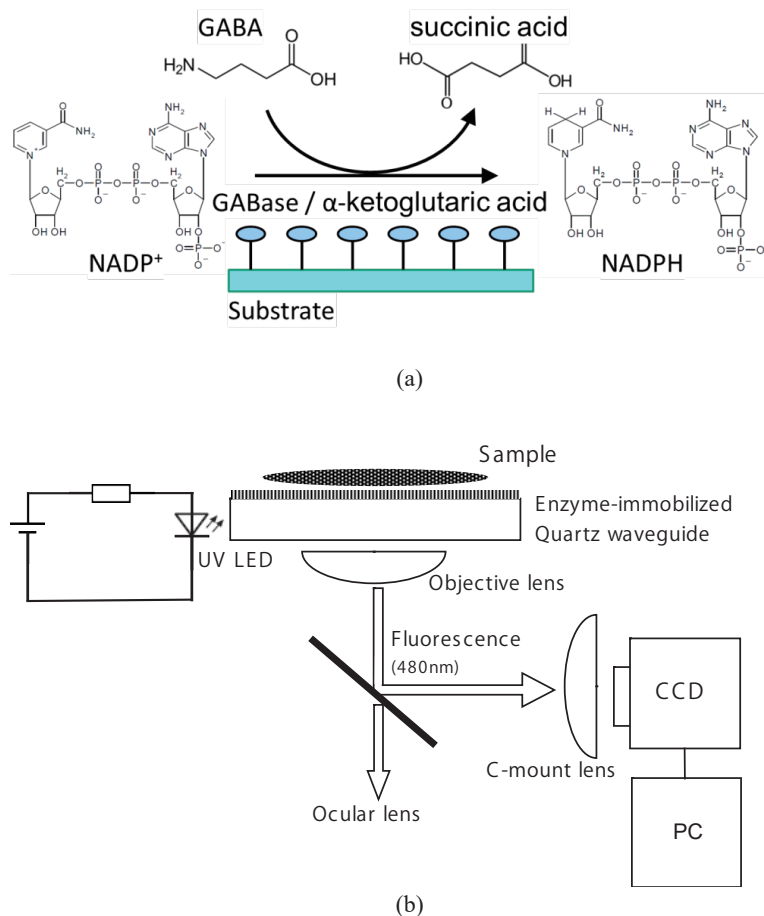


Fig. 1. (Color online) (a) Released neurotransmitters are oxidized by the oxidoreductase, and NAD(P)H is formed stoichiometrically. In GABA oxidation, released GABA is converted to succinic acid with NADPH formation by GABase. (b) Schematic diagram of the enzyme-linked photoassay system. The oxidoreductases are immobilized on the quartz glass surface, and the excitation light radiating from UV-LED passes through the quartz waveguide. Fluorescent images are obtained by CCD or CMOS, and analyzed using a computer system.

In some cases, glass surfaces were treated with either aromatic crosslinkers, 1,4-phenylene diisothiocyanate (1,4-DIC), or 1,3-phenylene diisothiocyanate [1,3-DIC, Fig. 2(b)], and glutaraldehyde (GA).⁽¹³⁾ Others were treated with a phosphonic acid, 11-aminoundecylphosphonic acid [11-AUPA, Fig. 2(c)], as a replacement for 3-APTS.⁽¹⁴⁾

Cerebellar acute slices were treated from postnatal day 3 (P3) to P15 in rats, sliced sagittally to a thickness of 400 μm with a rotor slicer (Dohan EM, Kyoto, Japan),

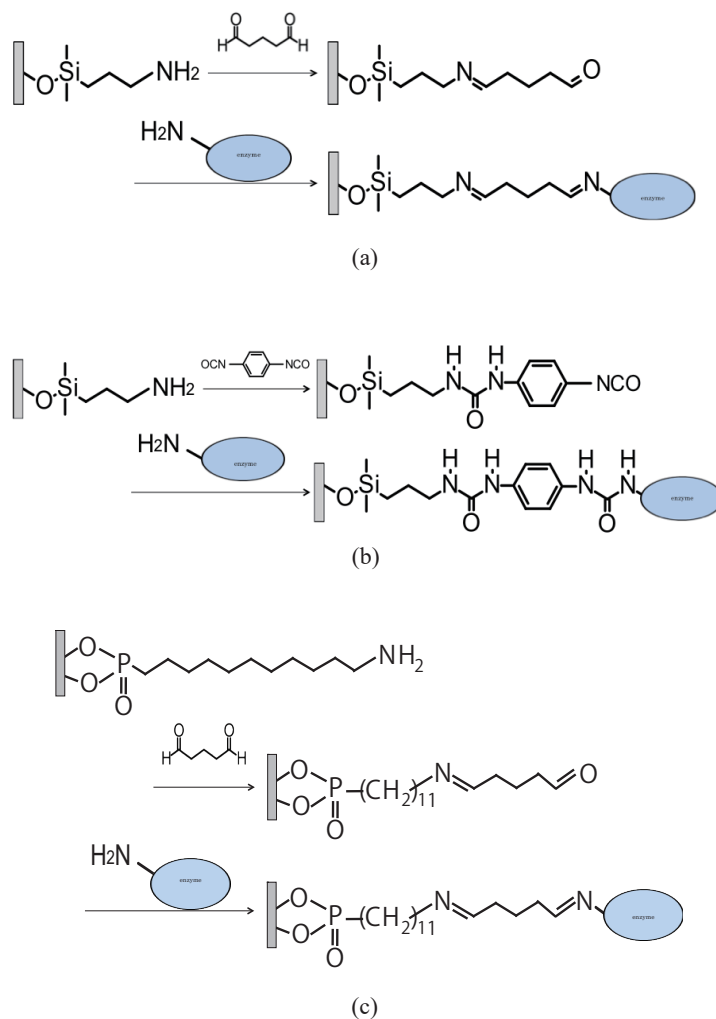


Fig. 2. (Color online) (a) Method of enzyme immobilization using 3-APTS and glutaraldehyde. Surface treatment and crosslinking between waveguide quartz and enzyme. (b) Crosslinking using 1,3-DIC. (c) Surface treatment with 11-AUPA.

and incubated in oxygen-aerated PBS for 45 min. All experimental procedures were approved by the committee for the use of animals at Toyohashi University of Technology and by the guidelines of the Ministry of Education, Culture, Sports, Science and Technology, Japan.

3. Results

3.1 *Spatiotemporal observation of glutamate release*

Figure 3(a) shows an illustration of rat cerebellar development. In the developing cerebellum, neuronal arrangement and circuit formation progress after birth. Granule cells, small input neurons, proliferate and migrate down from the external granular layer (EGL) to the internal granular layer (IGL). Purkinje cells, major output neurons, develop their dendrites and associate neuronal connections between granule cells and other interneurons. The layer of Purkinje cell somas is identified to be the Purkinje layer (PL). A neuronal circuit layer forms the molecular layer (ML).^(15,16) To understand the roles of neurotransmitters in the cerebellar development, we have developed a new visualizing device and, with it, we have observed spatiotemporal molecular dynamics.

Using the enzyme-linked photoassay system, we have observed many kinds of transmitter release in several developmental stages and organs. Our system has visualized both spontaneous and responsive transmitter release processes with 0.5 s time resolution. Figures 3(b)–3(k) show the transitions in glutamate release in response to 100 μM GABA application in developing cerebellar slices.⁽¹⁷⁾ Glutamate was released in both the EGL and the IGL, whereas the PL was indicated by a negative line. In the developing cerebellum, the granule cells that distributed in the EGL and IGL are the only neurons that release glutamate, so both layers showed fluorescence activities. Glutamate release in P3 cerebellar slices appeared in both layers slowly but continuously, whereas it started rapidly in the lower EGL and then spread to the IGL within a short time in P7 cerebellar slices.⁽¹⁸⁾ Granule cells in the P3 cerebellum did not develop sufficiently to react to GABA stimulation nor release the transmitter actively, but they still proliferated. On the other hand, the granule cells in the P7 cerebellum developed sufficiently to react to GABA stimulation, so they released glutamate rapidly.

Although spatiotemporal observation could give us dynamic information about neuronal reaction, our system needs to be improved in terms of stability, sensitivity and time resolution for us to observe fast synaptic transmissions. The targets of our improvements were the (1) sensing CCD, (2) excitation waveguide, and (3) manner of enzyme immobilization shown in Fig. 2.

3.2 *Effects of new crosslinkers and surface treatment*

Two types of glass devices with either aromatic crosslinkers, 1,3-DIC or 1,4-DIC, and GA were examined to observe spontaneous GABA release with 500 ms time resolution using ORCA ER CCD. The device formed using 1,3-DIC and GA gave images with a better contrast of GABA release than the GA crosslinked device in the P10 cerebellar slice [Fig. 4(a)], whereas it showed no difference in the P6 cerebellar slice. The 1,4-DIC crosslinked device yielded no good images.

The aromatic crosslinkers make the glass surface hydrophobic. Because mature brain tissues become hydrophobic as the myelin structure develops, 1,3-DIC crosslinking should increase the affinity of the enzyme for the tissues.

The binding between the glass and the acceptor molecules has been weak, because the silane coupling agents tend to undergo hydrolysis under biological conditions. The

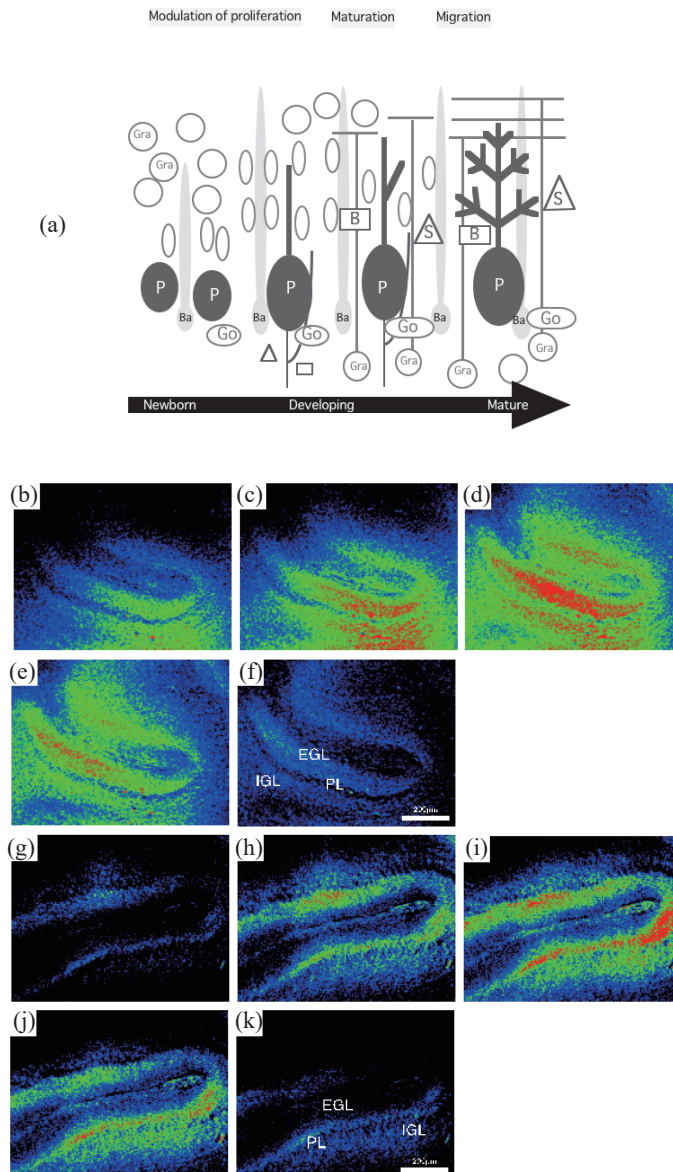


Fig. 3. (a) Diagram of cerebellar development. In the newborn cerebellum (1 to 3 days after birth), granule cell progenitors (Gra) proliferate in the EGL, while immature Purkinje cells (P) form the PL with Golgi cells (Go) and some Bergmann glia (Ba). During the development, 5 to 7 days after birth, Gra-cells elongate their axon and migrate inside, and P-cells spread their dendrites and connect to other neurons within two weeks. B denotes basket cells, and S, satellite cells. Evoked glutamate wave with GABA application in developing cerebellar cortex. (b)–(f): 2.0, 4.5, 7.0, 12.5, and 23.5 s after stimulation in P3 cerebellar cortex, respectively. (g)–(k): 0.5, 2.5, 4.0, 11.0, and 16.0 s after stimulation in P7 cerebellar cortex, respectively.

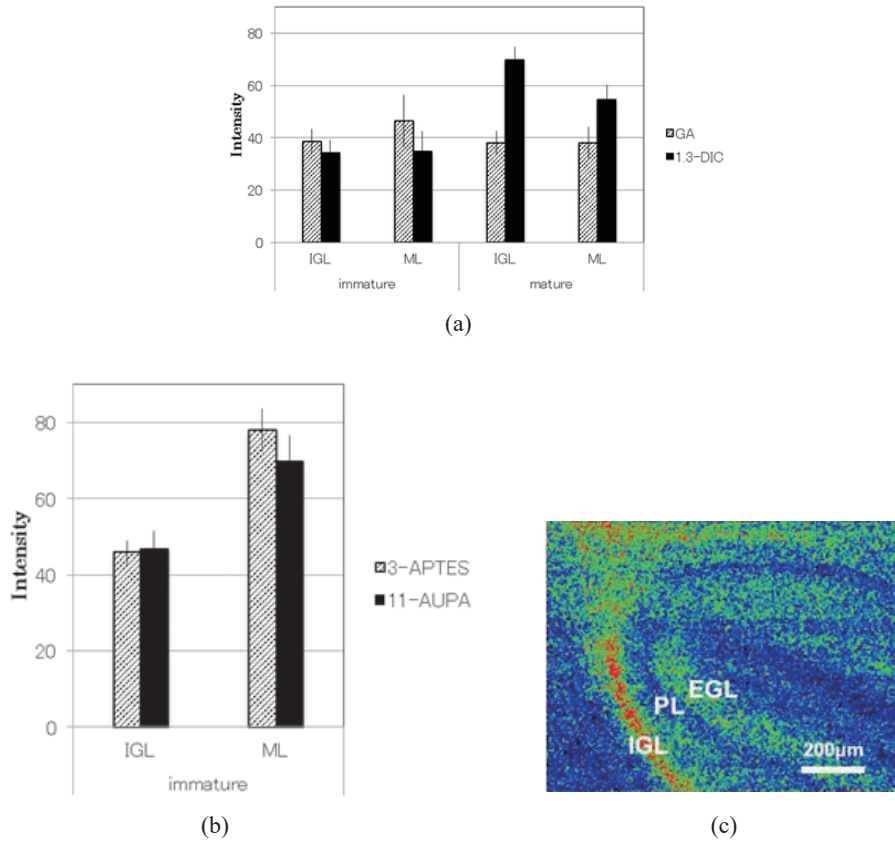


Fig. 4. (Color online) (a) New crosslinker, 1,3-DIC, gave us better contrast images than GA in mature cerebellar observation, while it made little difference from GA in immature organ. (b) The 11-AUPA-GA treatment showed the same result as the APTS-GA treatment in the immature organ. (c) Spontaneous GABA release image in P12 cerebellar slice using 1,3-DIC crosslinking glass device.

surface treatment by 11-AUPA, as a replacement for 3-APTS, was expected to inhibit hydrolysis, but it had low affinity for the glass. We constituted a new glass device with 11-AUPA-coupling enzymes and examined its sensitivity and stability. Figure 4(b) shows that the new device performed with the same sensitivity and stability as the device with APTS.

3.3 Observation using high-speed CMOS camera

The fluorescence intensity of NADH is very low and is only a few thousands of the intensity of typical artificial fluorescence. To collect data with sufficient time resolution, a highly sensitive and rapid data transferring camera is required. The time resolution

shown in Fig. 3 is 0.5 s for the 12-bit ORCA CCD, which is too low to detect the synaptic transmitter reaction.

A 16-bit CMOS camera, Flash 4.0, could detect weak light and transfer data in less than a microsecond. Using this camera, transient glutamate release could be detected with a 20 ms time resolution (Fig. 5). In developing the P7 cerebellum, glutamate release was increased in the EGL by applying a glutamate receptor-stimulating agent, α -amino-3-hydroxy-5-methyl-4-isoxazolepropionic acid (AMPA). Even in the premature P14 cerebellum, the increment in the rate of glutamate release was observed. It was not strong and noiseless, but the AMPA stimulation-induced glutamate release was observed in the ML and IGL where the glutamatergic neurons are distributed.

4. Discussion

The detection of neurotransmitter release gives us important information about developmental conditions and diseases. Parkinson's disease, a degenerative disorder of the central nervous system, is caused by the alteration of the release of neurotransmitters. The detection of the spatial or temporal alteration of the release would require early diagnosis and treatment of Parkinson's disease. In immature or lesioned neuronal organs, transmitters are released and taken up slowly, so the time resolution required is from 0.5 to 1 s. In young-adult stages, the release speed becomes higher than that in the immature stage within 20 ms.

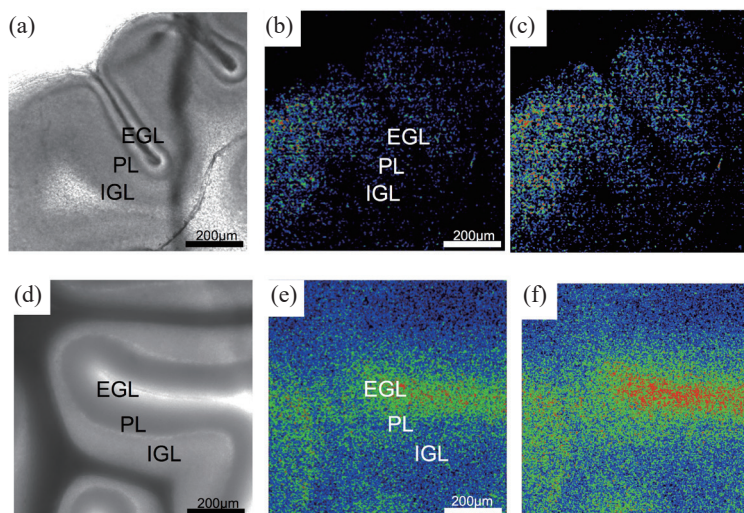


Fig. 5 (Color online) Evoked glutamate release images to AMPA stimulation for 20 ms time resolution using Flash 4.0 CMOS system. (a)–(c) P7 cerebellar slice; (d)–(f) P14 cerebellar slice. (a) and (d) Phase contrast light images. (b) and (e) Fluorescence images before stimulation and (c) and (f) just after AMPA stimulation.

Enzyme-linked assays were applied previously for chemical detection because of their specificity. In spatial observations, however, their fluorescence intensity is too weak to detect. Our enzyme-linked photodevice was developed to detect spatiotemporal neurotransmitter release, and it was improved to observe rapid synaptic release. New crosslinkers could contribute to a more sensitive detection, and the phosphonic surface treatment would expand the range of applications. In order to detect a high-speed transmitter release, both the light accumulation system for weak fluorescence and the close contact between the specimen and the enzyme are required. At present, our photodetection system detects several ms releases from neuronal synapses in the presence of noise, and in the future, it could give us more noiseless observations using an optimal image processing system.

5. Conclusions

The newly developed enzyme-linked photoassay is useful for the visualization of neurotransmitter release in brain slices. In the immature cerebellum, the granule cells release glutamate slowly or rapidly at their stage of neuronal development and synaptogenesis.

Using a fast new system, the rapid measurement of transmitter release in a young-adult cerebellar cortex became possible. Crosslinkers and other device techniques are required for stable observations. We suggest that the photoassay systems have advantages for the observation of synaptic release in several diseases.

Acknowledgements

This study was supported by grants from Scientific Research (C) 23500516 and 26350498, and Health Labor Sciences Research.

References

- 1 J. Moran and M. Rivera-Gaxiola: *J. Neurosci. Res.* **33** (1992) 239.
- 2 P. Varju, Z. Katarova, E. Madarasz and G. Szabo: *Cell Tissue Res.* **305** (2001) 239.
- 3 D. Casel, J. Brockhaus and J. W. Deitmer: *J. Physiol.* **568** (2005) 111.
- 4 M. Ochi, S. Shiozaki and H. Kase: *Neuroscience* **127** (2004) 223.
- 5 T. Morishima, M. Uematsu, T. Furukawa, Y. Yanagawa, A. Fukuda and S. Yoshida: *Neurosci. Res.* **67** (2010) 347.
- 6 T. Wang, T. Kumada, T. Morishima, S. Iwata, T. Kaneko, Y. Yanagawa, S. Yoshida and A. Fukuda: *Cereb Cortex* **24** (2014) 1088.
- 7 S. Yoshida and N. Hozumi: *JNNS* **20** (2013) 14.
- 8 H. Muramoto, Y. Sekino, N. Hozumi, A. Fukuda and S. Yoshida: 42th Neuroscience Meeting (2012) (CD-ROM).
- 9 B. Innocenti, V. Parpura and P. G. Haydon: *J. Neurosci.* **20** (2000) 1800.
- 10 M. Israel and B. Lesbats: *J. Neurochem.* **67** (1996) 2624.
- 11 S. Yoshida: Japanese Patent No. 4480952 (2010).
- 12 L. Blasi, L. Longo, PP. Pompa, L. Manna, G. Ciccarella, G. Vasapollo, R. Cingolani, R. Rinaldi, A. Rizzello, R. Acierno, C. Storelli and M. Maffia: *Biosens. Bioelectron.* **21** (2005) 30.

- 13 N. Aissaoui, J. Landoulsi, L. Bergaoui, S. Boujday and J. F. Lambert: *Enzyme Microb. Technol.* **52** (2013) 336.
- 14 M. Bariana, M. S. Aw, M. Kurkuri and D. Losic: *Int. J. Pharm.* **443** (2013) 230.
- 15 M. Yamada, M. Terao, T. Terashima, T. Fujiyama, Y. Kawaguchi, Y. Nabeshima and M. Hoshino: *J. Neurosci.* **27** (2007) 10924.
- 16 M. Ito: *The Cerebellum and Neural Control* (Raven Press, New York, 1984) Chap. 1.
- 17 M. L. Fiszman and A. Schousboe: *J. Neurosci. Res.* **76** (2004) 435.
- 18 K. Okochi, S. Hirano, K. Maruya, T. Morishima, C. Takayama, A. Fukuda and S. Yoshida: *J. Neurosci. Res.* **61** (2008) S114.

About the Authors

Kazunori Watanabe was born in Hokkaido, Japan, on February 3, 1992. He is a 2nd-year student in the Graduate School of Toyohashi University of Technology. His research focuses on the optimization of surface modifications for biosensors and the detection of neurotransmitters. He is a member of the Japan Neuroscience Society.

Nobuto Takahashi was born in Tokyo, Japan, on December 9, 1992. He is a 1st-year student in the Graduate School of Toyohashi University of Technology. His research focuses on bioengineering photoanalysis of cells and the developmental mechanism of cultured neurons. He is a member of the Japan Neuroscience Society.

Naohiro Hozumi was born in Kyoto, Japan, on April 2, 1957. He received his B.S., M.S., and Ph.D. degrees in 1981, 1983, and 1990, respectively, from Waseda University. He was at the Central Research Institute of Electric Power Industry (CRIEPI) from 1983 to 1999. He was an associate professor at Toyohashi University of Technology from 1999 to 2006, and a professor at Aichi Institute of Technology from 2006 to 2011. Since 2011, he has been a professor at Toyohashi University of Technology. He has been engaged mostly in research on insulating materials and diagnosis of high-voltage equipment and acoustic measurement for biological and medical applications. In 1990 and 1999, he received awards from IEE of Japan for his outstanding research papers. He is a member of IEEE, IEE of Japan, and the Acoustic Society of Japan.

Sachiko Yoshida was born in Toyama, Japan, on January 24, 1961. She received her B.S., M.S., and Ph.D. degrees in 1983, 1986, and 1990, respectively, from the University of Tokyo. She was a JSPS Postdoctoral Researcher from 1990 to 1992, a JST PRESTO Researcher from 1992 to 1994, and a research associate at Toyohashi University of Technology from 1995 to 1996. Since 1996, she has been a lecturer at Toyohashi University of Technology. Her research interests focus on physiological interaction and morphological transformation through brain differentiation, and their detection. She is a member of IEEE, International Brain Research Organization, the Society for Neuroscience, and the Japan Neuroscience Society.

Visualization of Spatially Distributed Bioactive Molecules using Enzyme-Linked Photo Assay

Hikaru Mabuchi* Student Member, HongYao Ong* Associate
Kazunori Watanabe* Non-member, Sachiko Yoshida* Non-member
Naohiro Hozumi*^{a)} Senior Member

(Manuscript received March 18, 2015, revised Oct. 4, 2015)

In this paper, we propose a new simple device for visualizing bioactive molecules with a fine spatial resolution by using a membrane in which a specific enzyme is immobilized. The layer produces fluorescence after association with a specific substance. The layer, on which a biological tissue is to be mounted, is deposited on a quartz substrate that is used as a light guide to introduce UV light to the layer. Substance release is observed by a CCD camera from the opposite side of the substrate. In order to shorten the experiment time, we had automated the optical device. The paper also describes the reduction of background fluorescence by means of image processing technique. Images were acquired by employing two UV-LEDs with slightly different angle. Image processing was performed to separate background and target fluorescence by means of independent component analysis. Finally the release of GABA(γ -aminobutyric acid) and glutamate from specific layers in rat cerebellum was successfully observed. It is expected that, using this method, both real-time transmitter release and its response to medicine can be observed.

Keywords : bioactive molecules, enzyme-linked photo assay, independent component analysis

1. Introduction

Light guide is composed of a dielectric material that can enclose the light propagation. In addition to being applied to communication, it is useful for sensing as well. In chemical sensing the surface of the light guide has to be coated with some specific chemical that may change its optical property depending on chemical reactions. Such a function can be applied to chemical imaging, if the light guide has a flat surface. This study proposes an application of two-dimensional light guide, of which surface is chemically modified, to biochemical imaging.

Neurotransmitter molecules released from neurons are not only regulators of neuronal transduction but also indicators of neuronal conditions. Glutamate and γ -aminobutyric acid (GABA) are known as typical transmitters in brain cortex that play important roles as stimulator and suppresser, respectively. Lack of balance in the release of glutamate and GABA may lead to autism, epilepsy or Parkinson's disease⁽¹⁾⁽²⁾.

In order to observe the spatio-temporal release in cerebellar cortex, we have newly proposed the enzyme-linked photo assay system, which is realized even using normal CCD camera, and observed GABA release in developing cerebellar slice using either new or authorized methods⁽³⁾.

In this paper, we propose a new simple device for this purpose by using a reactive layer in which a specific enzyme is immobilized, and produces fluorescence after association with a specific substance released from mounted slice. This layer is bound a quartz substrate that is used as a light guide for UV light

excitation. Fluorescence derived from a substance is observed by a CCD camera from the opposite side of the substrate.

The paper describes the reduction of background fluorescence by means of image processing technique. Finally it will be shown that the release of transmitters from specific layers in rat cerebellum was successfully observed.

2. Specimen Preparation and Photo Excitation System

Imaging of neurotransmitter release was monitored the reaction of oxidoreductases generating reduced nicotinamide adenine dinucleotide (NAD⁺) or diphosphonucleotide (NADP⁺). For glutamate and GABA, we used glutamate dehydrogenase and GABA disassembly enzyme (GABase), respectively.

Enzymes were covalently immobilized on the quartz glass substrate using a silane coupling agent and a crosslink agent. The substrate was as thick as 1 mm. Stoichiometrically generated NADH or NADPH emits 480 nm fluorescence after excitation at 340-365 nm.

Existence of glutamate and GABA lead to fluorescence when co-existing with specific enzyme and co-enzyme. A glass substrate on which specific enzyme is coated is in contact with the biological specimen. A chamber space is created around the specimen. The space is filled with buffer liquid and co-enzyme. On the glass substrate therefore, the specimen is in contact with both enzyme and co-enzyme.

Consequently glutamate or GABA, that is released from the tissue spontaneously by stimulation, makes an oxidation-reduction reaction on the substrate. Although both glutamate and GABA do not produce fluorescence by themselves, NAD(P)H that is created as the result of the above chemical reaction makes fluorescence. As the ratio of glutamate or GABA and NAD(P)H is 1:1, the

a) Correspondence to: Naohiro Hozumi. E-mail: hozumi@icceed.tut.ac.jp

* Toyohashi University of Technology
1-1, Hibarigaoka, Tenpaku, Toyohashi 441-8580, Japan

fluorescence can be correlated to the amount of released glutamate or GABA.

In the experiment, rat cerebellum was sliced sagittally at 400 μm thick and incubated in oxygen-aerated HEPES- Na^+ buffer for 40 min. The slice was placed on the quartz glass substrate with both NADP^+ and α -ketoglutarate. Figure 1 shows the schematic diagram of the observation system including the device. The enzyme was immobilized covalently on the glass as shown in Fig. 2. Figure 3 shows chemical reactions taking place on the substrate. NADP^+ (nicotinamide adenine dinucleotide phosphate) changes into NADPH (reduced nicotinamide adenine dinucleotide phosphate) just as glutamate and GABA degeneration. Synthesized NADPH was illuminated by 360 nm surface UV-LED, and emitted the 480 nm fluorescent light observed by cooled CCD (ORCA ER, Hamamatsu Photonics). The quartz substrate can be recognized as a light guide to illuminate the surface of the substrate.

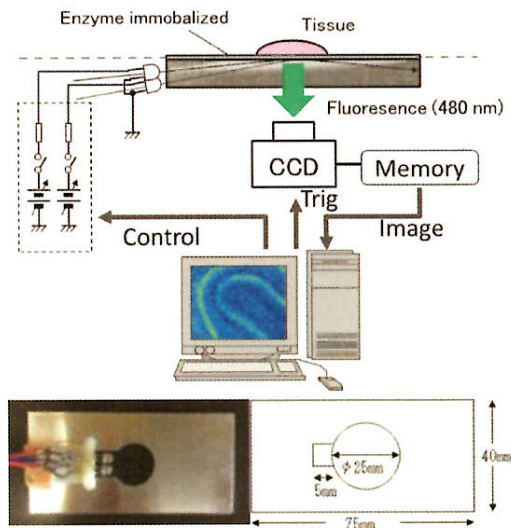


Fig. 1. Schematic diagram of the observation system including the device and its outlook

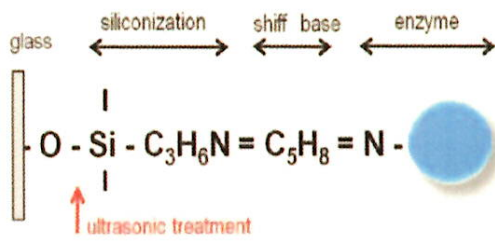


Fig. 2. Immobilized enzyme

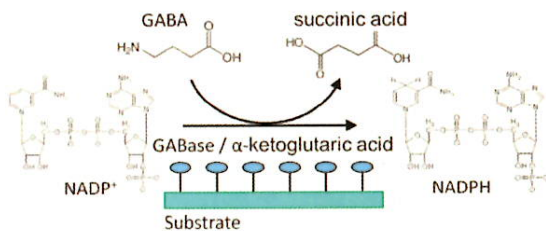


Fig. 3. Chemical reaction on the substrate

3. Image Processing

The fluorescent light detected by the CCD camera is divided into target light and background light. As significant intensity of background light is detected, it is assumed that fluorescence is excited by the light that is refracted on the interface between the substrate and tissue system including the layer. The light, being generated by LEDs and propagates through the substrate, can be decomposed into plane waves with different angles of propagation. Each plane wave transfers across the enzyme layer and comes into the tissue. We assume that both target and background light were predominantly excited by normal light. As the background light significantly damage the quality of the image, it should be reduced as much as possible. Making use of the evanescent light may be a solution, however, it may make the system complicated, and the target light may be not as significant as this case. Therefore we tried to reduce the background by means of a simple image processing.

Assuming that the light is a plane wave and scatter can be neglected, wave propagation and detected fluorescence can be illustrated as Fig. 4. In the figure, fluorescence, attributed to the layer where the enzyme is fixed, is represented as I_0 . This is

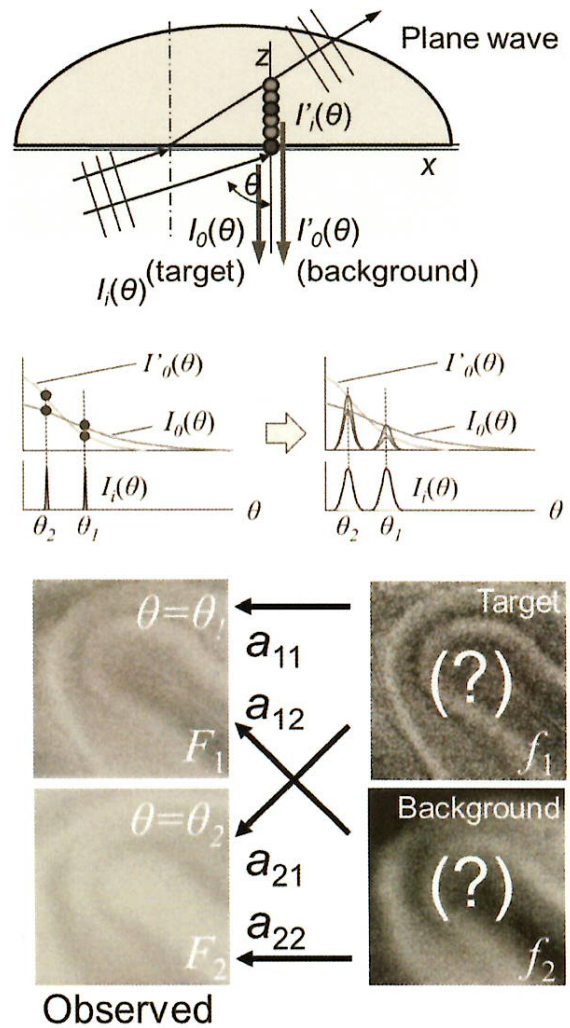


Fig. 4. Fluorescence detected by CCD camera

defined as to be the target. The fluorescence attributed to the tissue is represented as I_0 . This is defined as to be the background. Both I_0 and I'_0 depends on the incident angle θ . The thickness of the quartz plate, which is used as a light guide, is as thick as 1 mm. As it is much thicker than the diameter of normal optical fiber it is relatively easy to introduce two kinds of lights of which angles of center axes are significantly different. In addition, in practice, they depend differently on the incident angle. As the result, the proportion (I_0/I'_0) is not the same along θ . This is true even if the incident angle has distributed.

As the result, the captured fluorescence with different angle of optical axis is composed of target and background fluorescence with different mixture ratios. This can be represented as:

$$\begin{pmatrix} F_1 \\ F_2 \end{pmatrix} = \begin{pmatrix} a_{11} & a_{12} \\ a_{21} & a_{22} \end{pmatrix} \begin{pmatrix} f_1 \\ f_2 \end{pmatrix} \dots\dots\dots (1)$$

where $F_1(x,y)$ and $F_2(x,y)$ are captured fluorescence image, $f_1(x,y)$ and $f_2(x,y)$ are spatial distributions of fluorescence as the target and background, $a_{11}, a_{12}, a_{21}, a_{22}$ are constants. Although the image acquisition is sequential, ICA is performed by assuming that two images, $F_1(x,y)$ and $F_2(x,y)$ are acquired with a negligible time lag. Reproduced images $f'_1(x,y)$ and $f'_2(x,y)$ are calculated from F_1 and F_2 . As the result of periodical acquisitions of F_1 and F_2 , time dependent images of f'_1 and f'_2 are calculated. Eq. (1) can also be described using a matrix expression as:

$$\mathbf{F} = \mathbf{A} \cdot \mathbf{f} \dots\dots\dots (2)$$

The target and background fluorescence distribution can be calculated by applying \mathbf{A}^{-1} to \mathbf{F} . In practice, only contrast of the image would be enough to recognize the distribution. In such a case \mathbf{A}^{-1} can be represented as:

$$\begin{pmatrix} 1 & \alpha \\ \beta & 1 \end{pmatrix} \dots\dots\dots (3)$$

After capturing two images F_1 and F_2 by changing the angle of

optical axis, the target and background images can be separated by finding appropriate numbers for α and β . α and β can be tuned manually by monitoring the quality of reproduced image, however, the theory of independent component analysis (ICA) may be powerful for solving such a problem⁽⁴⁾.

Stochastic distribution of pixel intensity in images f'_1 and f'_2 are represented as $p(y_{1i})$ and $p(y_{2j})$, where y_{1i} and y_{2j} represent the intensity.

$$\left. \begin{aligned} p(y_1) &\equiv \{p(y_{11}), \dots, p(y_{1i}), \dots, p(y_{1n})\} \\ p(y_2) &\equiv \{p(y_{21}), \dots, p(y_{2j}), \dots, p(y_{2n})\} \end{aligned} \right\} \dots\dots\dots (4)$$

$p(y_{1i}, y_{2j})$ represents the probability that the intensity of a pixel in image f'_1 is y_{1i} and that of the corresponding point in image f'_2 is y_{2j} . In other words $p(y_1)$ and $p(y_2)$ are probabilities that cases y_1 and y_2 take place, respectively, and $p(y_1, y_2)$ is the probability that cases y_1 and y_2 takes place simultaneously. Variables y_1 and y_2 are considered to be independent when

$$p(y_1, y_2) = p(y_1)p(y_2) \dots\dots\dots (5)$$

is established. Kullback-Leibler(K-L) parameter is often employed to indicate the independency of variables:

$$KL \equiv \sum_{i,j} p(y_{1i}, y_{2j}) \log \frac{p(y_{1i}, y_{2j})}{p(y_{1i})p(y_{2j})} \dots\dots\dots (6)$$

The K-L parameter is zero when two sets of variables y_1 and y_2 are completely independent together. In practice, α and β in Eq. (3), which determine the probabilities $p(y_1)$, $p(y_2)$ and $p(y_1, y_2)$, can be tuned so that the K-L parameter indicates the minimum.

The process of ICA is illustrated in Fig. 5. The equation described in the form of matrix indicates that two images, F_1 and F_2 , derive from linear combination of unknown original images f_1 and f_2 . If an appropriate inverse matrix can be found then the original images can be reproduced. However as the matrix to describe the linear combination is unknown as well, ICA algorithm is applied to find the most appropriate matrix (as the inverse matrix). In the

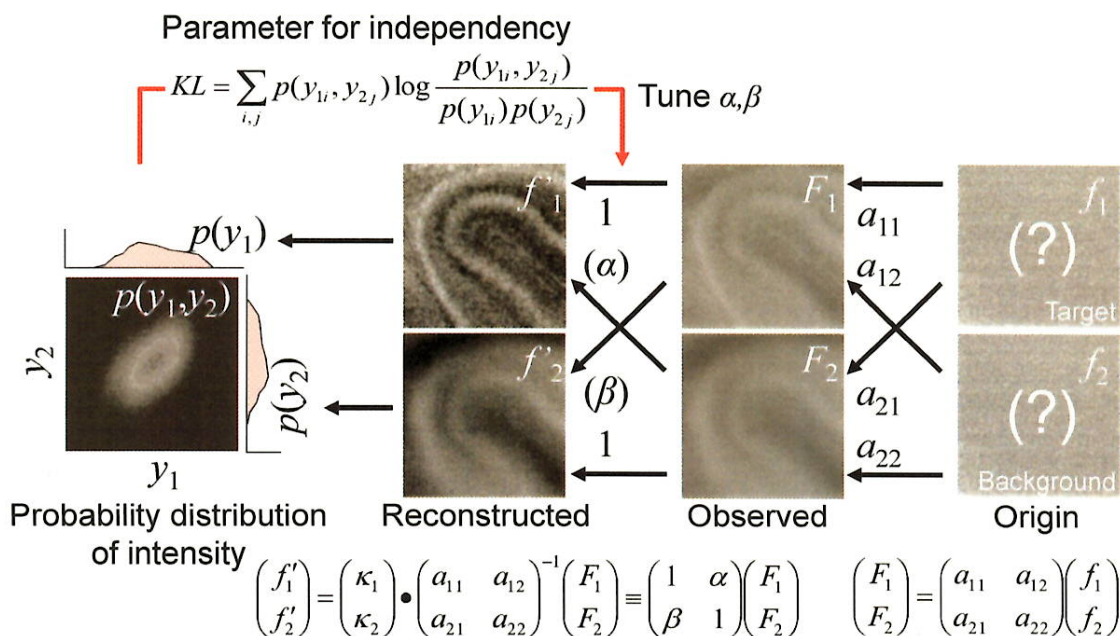


Fig. 5. Illustration for image processing based on independent component analysis

ICA process K-L parameter is calculated in order to evaluate the probabilistic independency of images f'_1 and f'_2 . It can be considered that in the reproduction algorithm the core process is the calculation of the K-L parameter. In this preliminary study K-L parameter is successively calculated by manually changing the inverse matrix, and images are assumed to be reproduced when the K-L parameter indicates the minimum.

4. Results and Discussion

4.1 Image Processing using the ICA Figure 6 (a) shows visible light image of the cerebellum with postnatal 21 days. In developing cerebellum, granule cells, small input neurons, proliferate and migrate down from the external granular layer (EGL) to the internal granular layer (IGL). As the development proceeds, EGL turns into molecular layer (ML) whereas IGL remains. Purkinje cells, big output neurons, develop their dendrites and associate neuronal connections between granule cells and other interneurons. Neuronal circuit layer forms the ML. As the cerebellum shown in Fig. 6 (a) is mature, ML, PL, IGL are clearly visible. Note that ML is on the outer side of the cerebellum, and a wrinkle surrounded by the ML is seen in Fig. 6 (a).

As for fluorescence observation, three different images were acquired. Two were with different inclination of the excitation

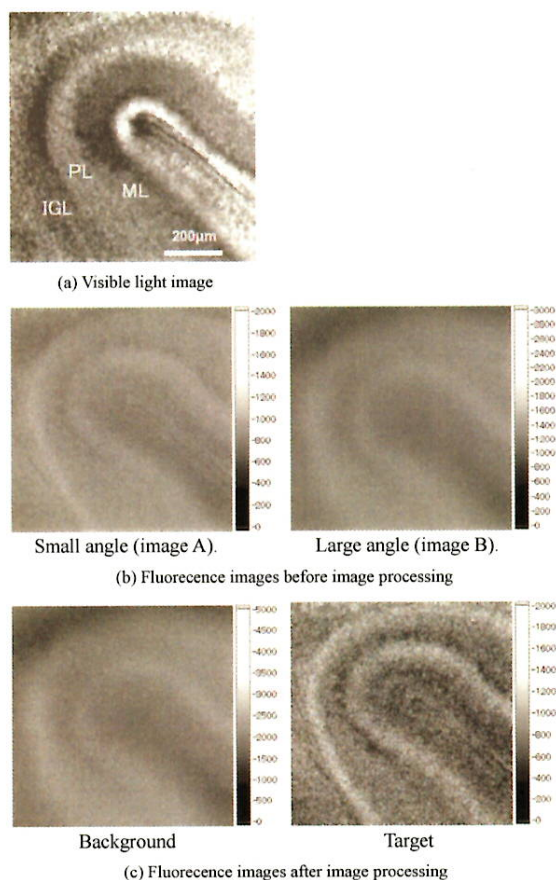


Fig. 6. Cross sectional images of cerebellar cortex: (a) Visible light image, (b) original fluorescent images with different angle of optical axes, and (c) fluorescent images after the image processing. Scales are indicated in arbitrary unit. Specimen: rat cerebellum (postnatal 21 days), target: GABA

light source, and one was with no excitation light. Each of the two images with excitation light was subtracted with the image with no excitation light, in order to reduce the background light from the outside. These two images after the subtraction were defined as images A and B.

Figure 6 (b) shows these images for a rat cerebellum. Both images are very unclear, because of the background fluorescence. Figure 6 (c) shows the result of image processing. It is clearly shown in the image entitled as “target” that the fluorescence intensity is high in two layers, whereas that entitled as “background” is not clear. By morphological inspection these layers are recognized as ML and IGL. These layers are known that GABAergic neurons distribute in mature cerebellum. Studies using HPLC and electrophysiological method have shown that GABA is released from the postnatal cerebellar cortex even before synaptogenesis, and that GABA receptors act on the developing cerebellar Purkinje cells⁽⁴⁾⁽⁵⁾. However, dynamic GABA release could not be observed unless the enzyme-linked photo assay is used. In addition, because cytoplasmic autofluorescence becomes noisy background light, it is useful that the image processing system extracted the image of GABA release from the autofluorescence-contained image. Using this method, both real-time transmitter release and its response to medicine can be observed.

4.2 Transition after Chemical Stimulation In relatively developed cerebellum, cells distributed in the ML and IGL are only the neurons of glutamate release, so that both layers showed fluorescent activities. Figure 7 indicates release distribution of glutamate in comparison with normal optical image illuminated with visible light. The fluorescent image, indicating glutamate release, is after the ICA processing. Figure 7 (c) indicates the regions of interest for analysis. Regions highlighted as ML and IGL have relatively strong intensity in fluorescence. They have a contrast to the region highlighted as PL. Release from white matter (WM), which is mostly composed of fatty materials, is much less significant.

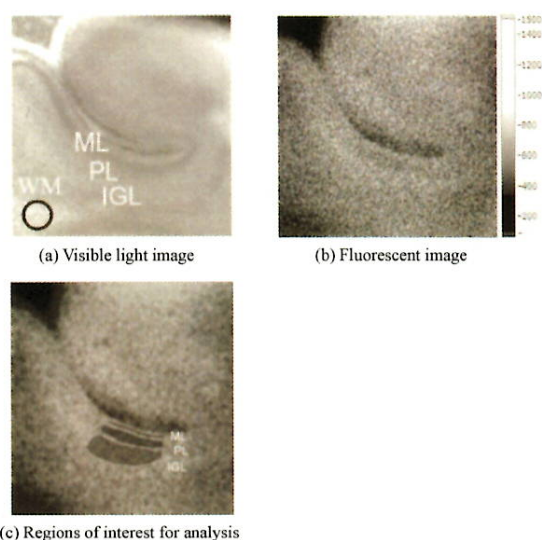


Fig. 7. Cerebellum with postnatal 7 days observed with visible light and fluorescent light indicating glutamate release. 0.9 mm × 0.9 mm. Gray scale is arbitrary. ML: molecular layer, PL: Purkinje layer, IGL: internal granular layer, WM: white matter. Specimen: rat cerebellum (postnatal 7 days)

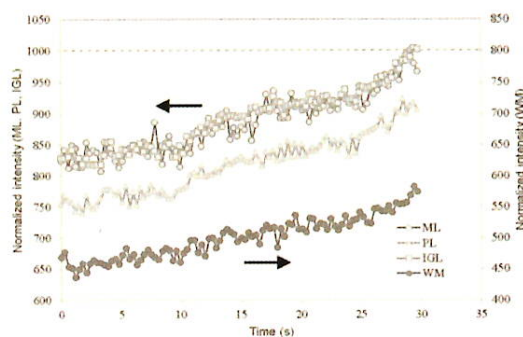


Fig. 8. Transition in fluorescence intensity in each layer (normalized by the intensity of ML 30 s after stimulation that is indicated as 1000). Specimen: rat cerebellum (postnatal 7 days), target: glutamate

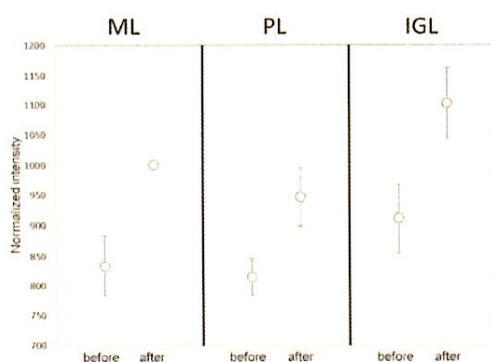


Fig. 9. Change in fluorescence intensity before and after AMPA stimulation (normalized by the intensity of ML 30 s after stimulation that is indicated as 1000). Specimen: rat cerebellum (postnatal 7 days), target: glutamate

Our system can visualize both spontaneous and responsive transmitter release with about 0.2 s time resolution. Figure 8 shows the transition of glutamate release in response to 100 $\mu\text{mol}/\ell$ (S)-alpha-Amino-3-hydroxy-5-methylisoxazole-4-propionic acid (AMPA) application in cerebellar slices. All values are normalized by the intensity of ML 30 s after stimulation that is indicated as 1000. Fluorescence, as indication glutamate release, was intense in both the IGL and ML, whereas the PL was indicated with lower intensity. As shown in Fig. 8, a clear increase in fluorescence was observed after stimulation. Transition in fluorescence was similar for ML and IGL, suggesting that these layers are activated. However PL, which was not expected to release glutamate, showed fluorescence as well although it was less intense than ML and IGL. As this specimen was taken from relatively young rat (postnatal 7 days), the cerebellar development was not totally completed, and the layers were not separated enough. It is hence considered that diffusion from ML and IGL to PL would take place, leading to an increase in fluorescence in this layer. The increase in fluorescence in WM suggests that glutamate might have been diffused into WM as well, although the absolute value was much lower than ML and IGL.

Figure 9 compares the fluorescence in each layer before and after stimulation. Four different specimens were used for the observation, in order to confirm reproducibility. It is clear that the AMPA stimulation brought a significant glutamate release from

ML and IGL, although the increase is also seen with PL.

5. Conclusions

A new method for visualization of spatially distributed bioactive molecules using enzyme-linked photo assay has been proposed. It is based on fluorescent reaction assisted by an enzyme immobilized on the substrate, however, background fluorescence disturbs the observation. In order to reduce the background fluorescence, two images were acquired by changing the optical axis of UV illumination. Image processing based on independent component analysis made the target image clear. Observation of rat cerebellum was successfully performed and GABA and glutamate release from two specific layers was clearly indicated.

Acknowledgement

The study was partially supported by grants from Scientific Research (C) 23500516, 26350498 and Health Labor Sciences Research.

References

- (1) N. C. Danbolt : "Glutamate Uptake", *Neurobiology*, Vol.65, pp.1-105 (2001)
- (2) N. Kasai, Y. Jimbo, O. Niwa, T. Matsue, and K. Torimitsu : "Real-time Multisite Observation of Glutamate Release in Rat Hippocampal Slices", *Neuroscience Lett.*, Vol.304, pp.112-116 (2001)
- (3) T. Morishima, M. Uematsu, T. Furukawa, Y. Yanagawa, A. Fukuda, and S. Yoshida : "GABA Imaging in Brain Slices Using Enzyme-linked Photo Analysis", *Neurosci. Res.*, Vol.67, pp.347-353 (2001)
- (4) V. Calhoun, G. Pearson, and T. Adali : "Independent Component Analysis to fMRI Data, A Generative Model for Validating Results", *VLSI Signal Processing*, Vol.37, pp.281-291 (2004)
- (5) F. F. Trigo, M. Chat, and A. Marty : "Enhancement of GABA Release through Endogenous Activation of Axonal GABA(A) Receptors in Juvenile Cerebellum", *J. Neurosci.*, Vol.27, No.46, pp.12452-63 (2007)
- (6) K. Obata : "Excitatory and Trophic Action of GABA and Related Substances in Newborn Mice and Organotypic Cerebellar Culture", *Dev Neurosci*, Vol.19, No.1, pp.117-119 (1997)

Hikaru Mabuchi



(Student Member) was born in Hokkaido, Japan on July 25, 1992. He is 1st-year student in Graduate School of Toyohashi University of Technology. His major is electric and electronic information. He has been engaged in research on bio-sensing by means of optical measurement. He is a student member of IEEEJ.

HongYao Ong



(Associate) was born in Malaysia on June 30, 1990. He received his B.S degree in 2014 from Toyohashi University of Technology, Japan. His major is electric and electronic information. He is currently engaged in GS Reality Sdn. Bhd., Malaysia. His major is electric and electronic information. He is an associate member of IEEEJ.

Kazunori Watanabe



(Non-member) was born in Asahikawa, Japan on February 3, 1992. He is 2nd-year student in Graduate School of Toyohashi University of Technology. His research focuses both the optimization of surface modification for biosensor, and detection of neurotransmitters. He is a member of Japan neuroscience Society.

Sachiko Yoshida



(Non-member) was born in Toyama, Japan on January 24, 1961. She received her B.S., M.S. and Ph.D. degrees in 1983, 1986 and 1990 from University of Tokyo. She was engaged in JSPS Postdoctoral Researcher from 1990 to 1992, JST PRESTO Researcher from 1992 to 1994, and Research Associate at Toyohashi University of Technology from 1995 to 1996. Since 1996, she has been a lecturer of Toyohashi University of Technology.

Her research interests focus the physiological interaction and morphological transformation through brain differentiation, and these detections. She is a member of a member of IEEE, International Brain Research Organization, Society for neuroscience, Japan neuroscience Society, and the Physiological Society of Japan.

Naohiro Hozumi



(Senior Member) was born in Kyoto, Japan on April 2, 1957. He received his B.S., M.S. and Ph.D. degrees in 1981, 1983 and 1990 from Waseda University. He was engaged in Central Research Institute of Electric Power Industry (CRIEPI) from 1983 to 1999. He was an associate professor of Toyohashi University of Technology from 1999 to 2006, and a professor of Aichi Institute of Technology from 2006 to 2011. Since

2011, he has been a professor of Toyohashi University of Technology. He has been engaged in the research in insulating materials and diagnosis for high voltage equipment, acoustic measurement for biological and medical applications, etc. He was awarded in 1990 and 1999 from IEE of Japan for his outstanding research papers. He is a member of IEEE, IEE of Japan and the Acoustic Society of Japan.